Integrated Master in Chemical Engineering

(Mestrado Integrado em Engenharia Química)

Microfluidic flow in porous medium analogues

Dissertation in Academic Environment

Evelien van Bokhorst

Universidade do Porto

Faculdade de Engenharia

FEUP

Department of Chemical Engineering

FEUP supervisor: **Manuel A. Alves**

FEUP co-supervisor: **Mónica S. N. Oliveira**

External co-supervisor (Delft Univ. Tech.): **Peter J. Hamersma**

February 12, 2010

Acknowledgements

I want to thank CEFT (Centro de Estudos de Fenómenos de Transporte) for providing the equipments and facilites to undertake this research project. I want to thank my supervisors, Mónica Oliveira and Manuel Alves for the very good guidance during the whole project. I also want to thank Peter Hamersma for arranging this project. Furthermore, I want to thank Patrícia Sousa for helping me with the experiments and answering my questions. And I want to thank Fernando Pinho for letting me use the master mold for the micro channels. Finally, I would like to thank ERASMUS for providing a scholarship.

Abstract

In this research project, the flow of complex (viscoelastic) fluids in microfluidic channels has been investigated experimentally. The microfluidic channels used were fabricated using soft lithography techniques and were composed of a series of contractions and expansions. Two distinct microchannel geometries, in a symmetric or in an asymmetric arrangement, were used in the experiments in order to mimic a porous medium.

The test fluids used were water and aqueous solutions of polyacrylamide (PAA) with different (dilute) concentrations. Detailed rheological measurements of the test fluids were done using shear and extensional rheometry. The PAA solutions were found to be elastic and to have a shear thinning behavior, which can be well described by a Carreau model. The effect of adding surfactant (SDS) and NaCl to the PAA solution was also studied and was found to reduce the shear thinning behavior substantially. In fact, addition of 1% NaCl confers the PAA solutions a behavior similar to that of a Boger fluid, in which the viscosity is nearly independent of shear rate, but still exhibits elasticity.

Pressure drop measurements were performed in addition to visualizations of the flow patterns by streak line photography for a wide range of flow rates. For the Newtonian fluid flows, inertia leads to the appearance of recirculations downstream of the expansion and the pressure drop increases linearly with the flow rate. For the viscoelastic fluids, recirculations appear upstream of the contraction due to elastic effects and two distinct behaviors are identified in terms of pressure drop. For the PAA solutions with additives at low flow rates, the pressure drop increases almost linearly with the flow rate as in the corresponding Newtonian case. Above a critical Deborah number (flow rate) there is a sudden increase in the pressure drop, which corresponds approximately to the onset of recirculations, due to an elastic instability. For the PAA solutions without additives a sudden increase in pressure drop is not observed and the relationship of pressure drop and flow rate is quasi-linear. A simple geometrical analysis and the use of Darcy's law demonstrated that the symmetric channel is a good approximation for a porous medium.

Key words: Microfluidics; Viscoelastic fluids; Rheology; Porous medium analogue.

Resumo

Neste projecto de investigação estudou-se experimentalmente o escoamento de fluidos complexos (viscoelásticos) através de microcanais com configurações análogas a meios porosos. Os canais usados foram fabricados usando técnicas de litografia suave que permitem obter geometrias com boa resolução espacial. Os canais são constituídos por uma sequência de contracções e expansões dispostas mediante duas configurações distintas: simétrica e assimétrica.

No trabalho experimental, utilizou-se um fluido newtoniano (água) e soluções aquosas de poliacrilamida (PAA) com diferentes concentrações. A reologia dos fluidos foi caracterizada em detalhe utilizando um reómetro de corte e um reómetro extensional. As soluções de PAA apresentam propriedades elásticas e um comportamento reofluidificante bem descrito por um modelo de Carreau. O efeito da adição de um surfactante e de NaCl à solução de PAA foi também estudada e observou-se uma redução substancial do comportamento pseudoplástico. De facto, a adição de 1% de NaCl às soluções de PAA confere ao fluido um comportamento semelhante ao de um fluido de Boger, cuja viscosidade é independente da taxa de corte, mas que exibe elasticidade.

Para a caracterização do escoamento, efectuaram-se medições de queda de pressão e visualizações do padrão de escoamento por fotografia com longos tempos de exposição para uma gama alargada de caudais. No caso do fluido newtoniano, a inércia leva ao aparecimento de recirculações a jusante da expansão e a queda de pressão aumenta linearmente com o caudal. Para os fluidos viscoelásticos, são observadas recirculações a montante da contracção devido a efeitos elásticos. Para estes fluidos, dois comportamentos distintos são identificados em termos de queda de pressão. Para as soluções de PAA com aditivos a baixos caudais, a queda de pressão aumenta quase linearmente com o caudal tal como acontece no caso newtoniano. Acima de um número de Deborah crítico, há um aumento súbito da queda de pressão, que corresponde aproximadamente ao aparecimento das recirculações a montante da contracção, devido a uma instabilidade elástica. Para as soluções de PAA sem aditivos, que apresentam um comportamento reofluidificante, não se verifica o aumento súbito da queda de pressão e esta varia quasi-linearmente com o caudal.

Finalmente, utilizando a lei de Darcy e uma análise geométrica simplificada, foi possível mostrar que o canal simétrico é uma boa aproximação a um meio poroso.

Palavras Chave: Microfluidica; Fluidos viscoelásticos; Reologia; Análogo de meio poroso.

Index

Notation and glossary

A	area	m^2
a	area of the cavity in the porous medium model	m^2
a_T	shift factor	-
D	characteristic dimension	m
d	particle diameter	m
f	friction factor	-
k	constant	cm^3/s
L	length	m
L_1	length of the experimental channel unit with large diameter	m
L_2	length of the experimental channel unit with small diameter	m
M	torque	N m
M_0	torque resolution	N m
n	power law index	-
Q	flow rate	m^3/s
R	radius	m
R_f	filament radius	m
r	radial distance	m
$\breve{R}$	parameter to define onset of secondary flow	-
T	temperature	K
T_{ref}	reference temperature	K
t	time	s
v	Velocity	m/s
v_c	velocity in contraction of the microchannel unit	m/s
W_1	width of the experimental channel unit with large diameter	m
W_c	width of the experimental channel unit with small diameter	m

Symbols

α	angle	rad
$\dot{\gamma}$	shear rate	s^{-1}
$\dot{\gamma}_r$	reduced shear rate	s^{-1}
ΔP	pressure drop	Pa
η	shear viscosity	Pa s

η_0	shear viscosity at a zero-shear rate	Pa s
η_∞	shear viscosity at an infinitely large shear rate	Pa s
η_{min}	minimum measurable viscosity	Pa s
η_r	reduced viscosity	Pa s
η_{ssf}	viscosity at which secondary flow starts	Pa s
κ	permeability	m^2
Λ_r	resistance factor	-
$\Lambda_{r,max}$	maximal resistance factor	-
Λ	time constant in Carreau model	s
ρ	density	kg/m^3
ρ_{ref}	reference density	kg/m^3
σ	shear stress	Pa
ω	angular velocity	rad/s

Dimensionless numbers

De	Deborah number	-
Re	Reynolds number	-
El	Elasticity number	-

Abbreviations

CAC	Critical Aggregation Concentration
PAA	Polyacrylamide
PDMS	Polydimethylsiloxane
PMMA	Polymethylmethacrylate
SDS	Sodium Docedyl Sulfate

1 Introduction

In the past, a major issue in industry was “how to scale up a process, which can be carried out in a laboratory, to a factory with a large capacity”. With the birth and development of chemical engineering as a field in the 19th and 20th centuries and advent of the industrial revolution this problem has been solved in the past one hundred years or so. For a few decades now, engineers have been facing the opposite problem: “how to scale down processes to a micro or even a nano scale?”. In electronics engineering this problem has already been solved fifty years ago with the invention of the microchip, which is now an essential component in day-to-day lives. In chemical, bio- and mechanical engineering the development of micro devices is still in an early stage. In the late sixties of the last century the first micro analytical device, a gas chromatograph, was designed by Brownlee and Silverstein (1968). Later, the silicon technology led to the invention of microelectromechanical systems (MEMS), and components like pumps, valves and sensors were developed at the micrometer lengthscale (Nguyen and Werely 2006). With these developments a new field emerged: microfluidics. Microfluidics is the science and technology of systems that process or manipulate small amounts of fluids (10^{-9} litres or less), using channels with dimensions of tens to hundreds of micrometres (Whitesides 2006). Microfluidics has applications in the chemical, biological, medical and electronic fields. The inkjet printer (Bassous et al. 1977) is an example of a microfluidics application which is widely used nowadays. Another example of a technology which would not exist without microfluidics is the lab-on-a-chip, in which different laboratory functions are miniaturized and integrated on a single chip. With this technology a set of (bio)chemical analyses can be performed on a microscale platform (Srinivasan et al. 2004; Weigl et al. 2003; Toner and Irimia 2005). There are many advantages in using these platforms at the microscale rather than the conventional macroscale equivalent: analyses are more precise, only a very small quantity of fluid is needed and the analysis apparatus is more practical (Merkerk 2005).

In this project, the focus is on the application of a microfluidics system for use as a simplified one-dimensional version of a porous medium analogue. It has been shown that the flow of viscoelastic fluids through porous media shows interesting and complex behavior due to the viscoelastic effects of the polymer (Marshall and Metzner 1967; Dauben and Menzie 1967; James and Mclaren 1975; Sorbie et al. 1987; Haas and Durst 1982; Bird et al. 1977; Kullicke and Haas 1984; Kozicki 2000). Understanding the behavior of these flows is important to make oil recovery procedures more efficient. Since soils like sand and clay have an average particle

size on the order of a hundred or a few hundred micrometers (international classification system of soil sizes), microchannels containing a series of contractions and expansions can be used as a simple porous medium analogue. The flow of diluted polymer solutions, which are commonly used for enhanced oil recovery, through microchannels will be studied.

1.1 Project outline

In this project, microchannels with two different geometries are used as simplified analogues for a porous medium. Diluted polyacrylamide (PAA) solutions will be used as working fluids. The goal is to describe the flow of a dilute polymer solution through the microchannels. In order to achieve this goal several experiments will be carried out. Shear and extensional rheology measurements will be done in order to characterize the fluids. Visualizations and pressure drop measurements will be performed in order to understand the flow of diluted polyacrylamide solutions through the microchannels.

1.2 Organization of the thesis

After this introduction, the thesis will start with a literature overview of experiments and applications of flows in microchannels and porous media. Next, the characterization of the fluid will follow in chapter three. In chapter four, the experimental procedures used for flow characterization will be described in detail and the results will be discussed. In chapter five the conclusions are written. The thesis will end with an evaluation of the project.

2 State of the art

2.1 Microfluidics

If the scale of a system is reduced, its complexity is increased (Raju and Roy, 2004) and several assumptions which are valid on the macroscale may not be valid on the microscale. On the macroscale the continuum hypothesis can be used to describe a liquid flow system, and properties like pressure, temperature, velocity and density are assumed to be well defined in an infinitively small volume (Bruus et al. 2008). Also the no-slip boundary conditions at walls are generally valid. Furthermore the flow is convective, and gravity and inertial effects play a major role in describing the fluid flow. On the microscale the continuum hypothesis and the no-slip boundary conditions may not be valid depending on the dimensions of the geometry and the fluid used. Dimensionless numbers can be used to determine if an assumption is valid in a given system – e.g., in gas flow, the Knudsen number can be used to determine if continuum or statistical mechanics are valid, and if no-slip or slip boundary conditions need to be used to describe the system (Bruus et al. 2008).

Flow at the microscale is typically laminar and, due to the reduced dimensions, viscous effects, surface effects, diffusion effects and, in some cases, even molecular effects play a major role (Nguyen and Wereley, 2006). The Reynolds number is used to determine if viscous or inertial effects are dominant in the system. The Reynolds number is defined by:

$$Re = \frac{\rho v D}{\eta} \tag{2.1}$$

where ρ is the density of the fluid (kg/m^3), v the velocity (m/s), D the characteristic dimension of the geometry (m) and η the viscosity (Pa s).

If $Re >> 1$ inertial effects are dominant over viscous effects, while if $Re << 1$ viscous effects are dominant over inertial effects. In the case of micro devices, the characteristic length scale is very small and very low Reynolds numbers can be achieved. The advantage of very low Reynolds numbers is that there is a purely viscous flow and inertial effects can be neglected.

On the other hand high deformation rates can be obtained in microfluidics, and elastic effects become important in fluids that would otherwise behave as Newtonian fluids in the equivalent macroscale flows (Groisman and Quake 2004; Rodd et al. 2005; Sousa et al. 2010). The Deborah number can be used to assess the elasticity of a certain fluid flow and is defined

as the ratio of the relaxation time of the fluid and the characteristic time scale of the flow. In section 4.6 the dimensionless numbers used in this thesis will be defined.

The flow of fluids through microchannels has been studied by many researchers throughout the years. With Newtonian fluids it turned out there are only slightly differences with conventional macro flow. Non-Newtonian fluids are more complex to describe on microscale due to their shear rate dependent viscosity and elastic effects (Barnes 2000). The nature of the flows changes in some cases from a simple shear flow to a complex extensional flow. In extensional flow polymer chains go from stretched to unstretched. The elasticity of the fluid, which is defined with the relaxation time, is an important property here. Since non-Newtonian fluids have elastic effects in addition to viscous effects, like shear thinning, it is particularly difficult to study extensional flows. David Boger discovered in 1977 the so called Boger fluids (Boger 1977). These fluids have a viscosity which is shear independent and therefore fluid elasticity is isolated from shear-thinning effects which simplifies the analysis of elasticity-driven phenomena. Boger fluids are most of the time highly diluted polymer solutions in a viscous solvent and have a high viscosity.

In previous studies the extensional flow of Boger fluids and shear thinning fluids has been extensively studied (Nguyen and Boger 1979; Evan and Walters 1986; Rothstein and McKinley 1998; Alves et al. 2005; Sousa et al. 2009, 2010; Groisman and Quake 2004; Rodd et al. 2005, 2007; Scott 2004; Oliveira et al. 2008; Arratia et al. 2006; McKinley et al. 2007; Groisman et al. 2003) Two types of experimental techniques for studying these extensional flow can be distinguished. Flow visualizations are a common method to study the vortex behavior of fluids through microchannels. Previous studies relate the flow patterns to dimensionless numbers (Reynolds, Deborah or Weissenberg number and Elasticity numbers) and observed several regions of flow behavior (Rodd et al. 2005). To validate the flow behavior simulations were done by Oliveira et al., 2008 among others.

Pressure drop measurements are another experimental technique which can give an insight into developing polymeric stresses in a contraction expansion flow (Rothstein and McKinley 1998). In previous studies with viscoelastic fluids a non linear relation of pressure drop and flow rate is observed. This effect can be attributed to elastic effects and the onset of flow instabilities.

2.2 Microchannel fabrication

Microchannels can be fabricated using several methods and materials. In the early years of microfluidics, glass was often used as a fabrication material. As glass manufactured microchannels were expensive, various alternatives have emerged since then, including "soft-technologies" that use polymers, such as polymethylmethacrylate (PMMA) and polydimethylsiloxane (PDMS), as main materials (Nguyen and Werely 2006). Besides the low cost, these materials offer enhanced versatility as there is a variety of polymers with different characteristics and surface chemistry. As such, the polymer used to fabricate a microfluidic device can be chosen depending on its applications. In the following sections two of the most widely used methods of microfabrication will be described: photolithography, which is commonly used to fabricate microchannels directly or to fabricate masters to be used in replication methods; and a replication method called soft-lithography developed by Xia and Whitesides (1998). For further details on these and other methods of fabrication refer to Nguyen and Werely (2006) and references therein.

2.2.1 Soft lithography

In this method, microchannel fabrication starts with the manufacture of a master mold. A common method to produce this mold is photolithography. Figure 2.1 shows the typical steps involved in the photolithography method. First, a semiconductor wafer is coated with a photoresist (step 1). The coated wafer is then exposed to UV-light through a photomask (step 2). The mask has a pattern so that the wafer is only exposed on the required places. After that, a developer is used to dissolve the exposed or unexposed regions of the photoresist.

The wafers are often made of silicon, but since this is a rather expensive material other alternative materials have been investigated for the same purpose. PMMA turned out to be a good substrate too (Bubendorfer et al. 2007).

Wafer coating can be done with a negative or a positive photoresist. A positive photoresist is insoluble in the developer, but exposure to UV light will cause a chemical change that makes the resist soluble in the developer. A negative photoresist is soluble in the developer, but will become insoluble when exposed to UV light. A commonly used photoresist is SU-8, a negative resist developed by IBM (Lorenz et al. 1997; Li et al. 2003; Zhang et al. 2001). The main advantage of this photoresist is its ability to achieve a high degree of crosslinking after exposure, which results in good side-wall resolution (Bubendorfer et al. 2007).

Furthermore, it is thermally stable, chemically resistant and has good mechanical properties (Feng and Farris 2003).

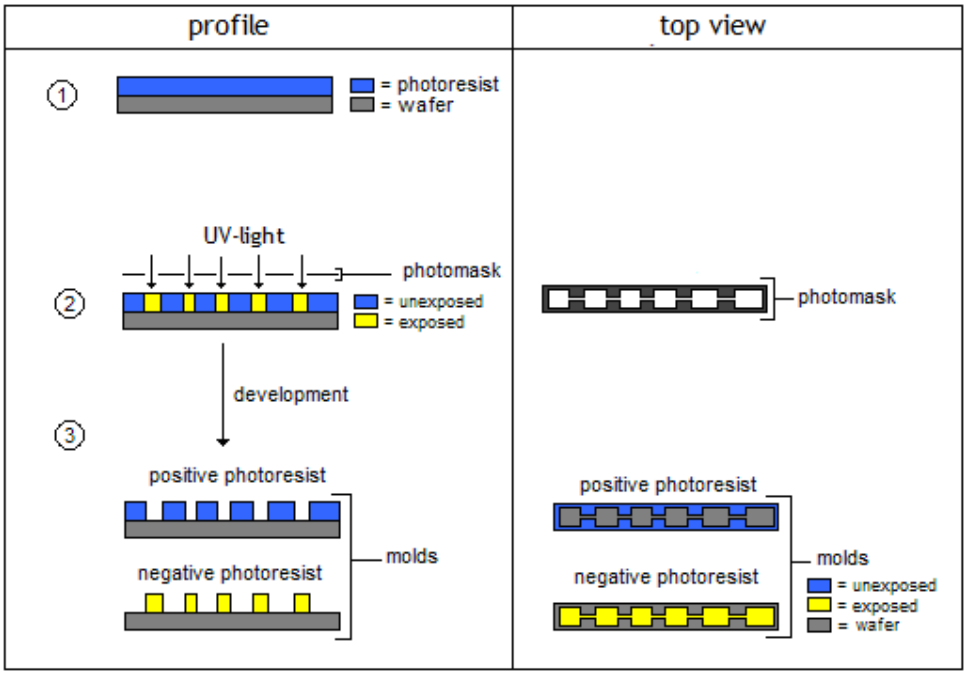

Figure 2.1: Mold fabrication using photolithography (Xia and Whitesides 1998).

With soft-lithography there is a limit on the aspect ratio (ratio between resist thickness and smallest dimension of channel) of approximately 25:1 (Bogdanov and Peredkov,2000). This is due to diffraction and absorption of the UV-light. In order to decrease this diffraction, X-ray radiation can be used in X-ray lithography or deep X-ray lithography (Becker et al. 1986). Since X-ray radiation has shorter wavelengths than UV light there will be less diffraction, and aspect ratios up to 100:1 can be achieved (Bogdanov and Peredkov 2000). Nevertheless, there are also problems with using X-ray lithography, such as the lack of a suitable photomask, defects in the mask and costs of the required tools (Peckerar and Moldanado 1993).

After the mold is ready, it can be used countless times to fabricate the polymer microchannels. First, the master mold needs to be silanized in order to make it easier to peel off the polymer in latter steps (Xia and Whitesides 1998). The polymer and curing agent are mixed, degassed and poured into the mold. The curing process is done by baking the mold and polymer at room temperature for several hours or at high temperatures using an oven or a hot plate for shorter times. After that, the polymer can be cut and peeled off the mold. The channels are then sealed by adhesion to a glass slide.

Polydimethylsiloxane is a polymer that exhibits interesting properties for use in soft lithography (Xia and Whitesides 1998; Becker and Locascio 2002; Scott 2004). PDMS is chemically stable, which means it will not react with many other polymers that might be flown through the channels later on. PDMS is impermeable to liquids and permeable to gasses. So, if air bubbles incidentally come into the microchannels they can be forced to permeate through the walls. PDMS has a good optical transparency that is essential in flow visualizations. It is a soft elastomer, which makes it flexible and has the added advantage of not breaking. PDMS exhibits good adhesion properties to rigid materials, which is useful when microchannels need to be sealed with glass plates. Furthermore PDMS is thermally stable up to 186°C, which makes it possible to cure thermally (Harper 1992).

Despite the numerous advantages, there are also some problems in using PDMS. The fact that PDMS is a flexible elastomer can also be a disadvantage. At high flow rates, pressure will be high and this can result in the expansion and deformation of the channels. The softness of PDMS also limits the channel aspect ratio (AR = depth of the channel/smallest characteristic dimension). If aspect ratios are too low sagging can occur, and if they are too high this can result in pairing (Xia and Whitesides 1998). Furthermore PDMS is hydrophobic which makes it difficult to wet the whole surface of the channel and frequently results in air bubbles trapped in corners (Xia and Whitesides 1998; Scott 2004).

2.2.2 Photolithography

Another method used to produce microchannels is photolithography. This method is similar to the mold fabrication process in soft lithography but in case of spincoating with photoresists here a thicker layer is coated onto the wafer. SU-8 is a photoresist typically used in photolithography since it has a very low optical absorbance in the UV-region. Therefore a uniform exposure of the UV light can be achieved resulting in vertical sidewalls (Lorenz et al. 1997).

Liu et al. (2003) describe a method to make microchannels with positive and negative photoresists. A positive photoresist is coated onto a substrate in a specific pattern. UV light or X-ray radiation are used for exposure and the exposed positive photoresist is removed, resulting in high precision microchannels. Subsequently, a negative photoresist (SU-8) and/or a glass plate are used to cover the structure and seal the system.

Both methods have advantages and disadvantages. Soft lithography is simple, low in cost and rapid prototyping is possible (Xia and Whitesides, 1998). The main disadvantages of this method are the deformation of the channels at high flow rates caused by the use of elastomers and the difficulty in the fabrication of complex structures. Using photolithography, microchannels with highly precise, complex and even 3D structures can be fabricated (Liu et al. 2003). However, with this method costs are high, prototyping is slower than with soft lithography and difficulties arise in the removal of SU-8.

2.3 Porous media

A medium which contains interconnected cavities can be defined as a porous medium. Porous media appear in several fields of science and engineering. In some fields, the porosity of a material/medium is an important property which needs to be considered and characterized, e.g. concrete in civil engineering, and soil in environmental and petroleum engineering. In other fields, a porous medium may be used to improve a process or system. In chemical engineering for example porous media appear as packed beds and are used in distillation columns or as reactors. A detailed understanding of the transport of fluids, heat and momentum through porous media is essential for a correct operation and improvement of applications using this type of flow. However, since typically porous media have non-homogeneous properties, such as porosity ($\varnothing$ = volume of voids/total volume of medium) and permeability, it is difficult to describe the transport processes.

In 1856, Henry Darcy investigated the flow of water in sand beds which lead to Darcy's law (Darcy 1856):

$$Q = \frac{-\kappa A}{\eta}\frac{\Delta P}{L} \tag{2.2}$$

where Q is the flow rate (m^3/s), κ the permeability of the medium (m^2), A the surface area (m^2) and ΔP the pressure drop (Pa) across a porous medium of length L (m).

Since Darcy's seminal work, the flow of fluids through porous media has been studied by many researchers. The studies of Forchheimer (1901), Brinkman (1947) and Ergun (1952) among others, lead to extensions of and deviations to Darcy's law.

The flow of non-Newtonian fluids through porous media is also an interesting subject of study (Marshall and Metzner 1967; Dauben 1967; James and McLaren 1974; Sorbie and Clifford 1987;

Haas and Durst 1982; Bird et al. 1977; Kullicke and Haas 1984 and Kozicki 2000). It has been shown that the flows of non-Newtonian fluids show an interesting behavior. Above a certain flow rate, a substantial increase in pressure drop is observed. This increase is due to an increase in flow resistance which is induced by viscoelastic effects. The Reynolds number, the Deborah number and the friction factor are important parameters in the characterization of these effects, i.e. to identify the onset of elasticity driven effects and explain the enhancement in pressure drop (Marshall and Metzner 1967). If parameters such as the Deborah number exceed a critical value, elastic effects will occur. Marshall and Metzner (1967) found that there are measurable pressure drop increases with Deborah numbers around 0.05 and an order of magnitude difference was observed with Deborah numbers around 1. Bird et al. (1977) found that the critical Deborah number is 0.5 for the onset of elastic-driven instabilities in extensionally dominated flows. Kullicke and Haas (1984) studied the critical values of the parameters above for flows of diluted polyacrylamide through packed beds and porous media. They defined a friction factor f and a resistance factor Λ_r $(=f \cdot Re)$ and have reached the following conclusions:

- a smaller particle diameter causes lower Re_{crit}, but $\Lambda_{r,max}$ will remain approximately the same;
- the molecular weight has to be very high in order to observe the onset of elastic effects;
- the polymer concentration only influences the resistance factor but the onset of the elastic effects will remain the same;
- the temperature and the solvent used also influence the onset of elastic behavior.

More recently, Yilmaz et al. (2009) studied the pressure drops of highly dilute polyacrylamide solutions (5 and 10 ppm) through a porous bed and found a power law relation between the flow rate and pressure drop ($Q = k \cdot \Delta P^n$ with $k = 10^{-5}$ cm^3 s^{-1} kPa$^{-1.1615}$ and $n = 1.1615$).

2.3.1 Applications

The flow of Newtonian and non-Newtonian fluids through porous media have an important application in petroleum engineering (Yilmaz et al. 2009). Oil is becoming a scarce fuel and therefore new processes to obtain oil need to be found. Enhanced oil recovery is a technique in which the amount of extracted oil is increased substantially. By using a tertiary recovery technique, 30-60% of the oil which is present in a reservoir can be extracted. In contrast, primary recovery usually amounts to only 10% and secondary recovery amounts to approximately 20-40% (according to the US department of Energy). An efficient method of enhanced oil recovery is polymer flooding, in which the reservoirs are injected with water

containing a low concentration of water-soluble-polymers with a high molecular weight. The polymers will cause an increase in the fluid viscosity and therefore will be able to push more oil out of the reservoir than water alone would. Polyacrylamide was shown to be a good polymer for this purpose (Yilmaz et al. 2009). PAA is a high molecular weight polymer which presents a high viscosity and elasticity at low concentrations. Furthermore, (hydrolized) polyacrylamide has long polymer chains due to repulsive effects which also lead to a higher viscosity. One of the disadvantages of using PAA is that at high shear rates, the polymeric solutions will be irreversibly degraded which leads to lower viscosities.

3 Fluid characterization

3.1 Fluid composition

A Newtonian (deionized water) and various viscoelastic polymeric solutions were used in this work. The polymer which is used throughout the experiments is polyacrylamide (Polysciences Inc.). This is a polymer with a high molecular weight ($18 \cdot 10^6$ g/mol).The concentrations which are used (50 and 125 ppm) are below the overlap concentration c^*, as shown in Sousa et al. (2010). This means that the polymer chains can be seen as independent of each other.

Aqueous solutions of polyacrylamide with concentrations of 50 and 125 ppm were prepared by diluting a stock solution (0.0018 g PAA/g solution). An ionic surfactant (sodium dodecyl sulphate, SDS, Sigma-Aldrich) was added in order to minimize the adhesion of fluorescent tracer particles, which are required for flow visualization experiments (cf. section 4.7), to the channels walls. Furthermore, a salt (sodium chloride, NaCl) is added to make the fluid neutrally charged and to minimize shear-thinning effects of shear viscosity.

After preparation, the fluids are mixed for a few hours with a magnetic stirrer at a very low angular velocity. If the velocities are high, polymer chains might break which will result in a different fluid rheology. By working with diluted polymer solutions, attention needs to be paid on the degradation of the polymer and, as such, high shear rates and high temperatures need to be avoided.

3.2 Shear rheology

In order to characterize the fluid rheology under steady shear, the shear viscosity is measured as function of the shear rate. The measurements were carried out at different temperatures (10, 15, 20 and 25°C) to evaluate the effect of temperature on the shear viscosity. Since additives are added to the solutions, their influence was also evaluated. In order to assess experimental repeatability, the same test is performed several times.

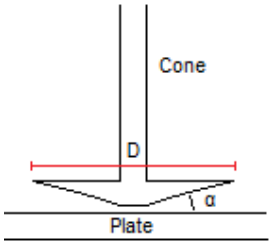

Figure 3.1: A cone and plate geometry.

3.2.1 Experimental Technique

The device which is used to measure the shear viscosity is a shear rheometer (Physica MCR 301, Anton Paar). A geometry is coupled to the apparatus and applying a torque creates a rotational movement that imposes a shear or stress on the sample. Different geometries can be used depending on the sample which needs to be characterized. To measure the shear viscosity of water and the viscosity of the dilute non-Newtonian fluids a cone-and-plate geometry was used. The advantage of using a cone-and-plate geometry relative to the plate-plate set up is as follows. With a cone-and-plate geometry (Figure 3.1) a uniform shear rate can be achieved throughout the sample (Raha et al. 1968), while in a plate-plate geometry this is not the case and the shear rate varies along the radius of the plate, R (cf. Appendix B).

The shear viscosity is measured as function of the shear rate. First, a shear rate is applied on the sample by giving the cone a set rotational speed through application of a constant torque. The sample resists to movement and creates a resistive torque, which is used to calculate the shear stress by:

$$\sigma = \frac{3M}{2\pi R^3} \tag{3.1}$$

where σ is the shear stress (Pa), M the torque (N m) and R the radius of the cone (m). The viscosity can now be calculated by:

$$\eta = \frac{\sigma}{\dot{\gamma}} = \frac{3M}{2\pi R^3}\frac{\alpha}{\omega} \tag{3.2}$$

with η the shear viscosity (Pa s), $\dot{\gamma}$ the shear rate (s^{-1}), α the cone angle (rad) and ω the angular velocity (rad/s).

The test procedures and the parameters adopted for a correct measurement of steady shear viscosity are discussed in detail in Appendix A.

3.2.2 Reliability region

To establish the domain in which viscosity measurements can be considered reliable two lines are drawn corresponding to fifty times the minimum torque and to the onset to secondary flow.

The minimum torque line is given by:

$$\eta_{min} = \frac{3M_0}{2\pi R^3 \dot{\gamma}} \tag{3.3}$$

where η_{min} is the minimum measurable viscosity (Pa s), M_0 the torque resolution of the rheometer (N m). The used device has a torque resolution of $1 \cdot 10^{-7}$ N m.

The measured points which are left from this line are not considered valid because the equipment does not give accurate results in this domain. In fact, only the points to the right of the line corresponding to 50 times the minimum torque, which corresponds to a maximum error of 2% in the shear viscosity, are considered.

The line corresponding to the onset of secondary flow due to inertial instabilities can be calculated by (Sdougos et al. 1984)

$$\eta_{ssf} = \frac{R^2 \omega \alpha^2 \rho}{12\breve{R}} \tag{3.4}$$

with η_{ssf} as the viscosity at which **s**econdary **f**low will **s**tart (Pa s) and $\breve{R}$ as a parameter ($\breve{R}$ = 0.5 for onset of secondary flow)

The line corresponding to the onset of secondary flow depends on the density of the fluid, but since this property does not change significantly for the fluids used (cf. Table 3.3) and the lines almost overlap, only one line corresponding to the density of water at 20°C, ρ = 998.2 kg/m^3, is shown in the shear viscosity figures.

Furthermore, for the PAA solutions the viscosity for high shear rates shows a considerable increase, which is attributed to elastic instabilities rather than inertial driven secondary flow. These elastic instabilities produce an increase in the measured torque which is translated as an increase in viscosity. Figure 3.2 gives an example of a flow curve with the minimum torque and secondary flow lines shown.

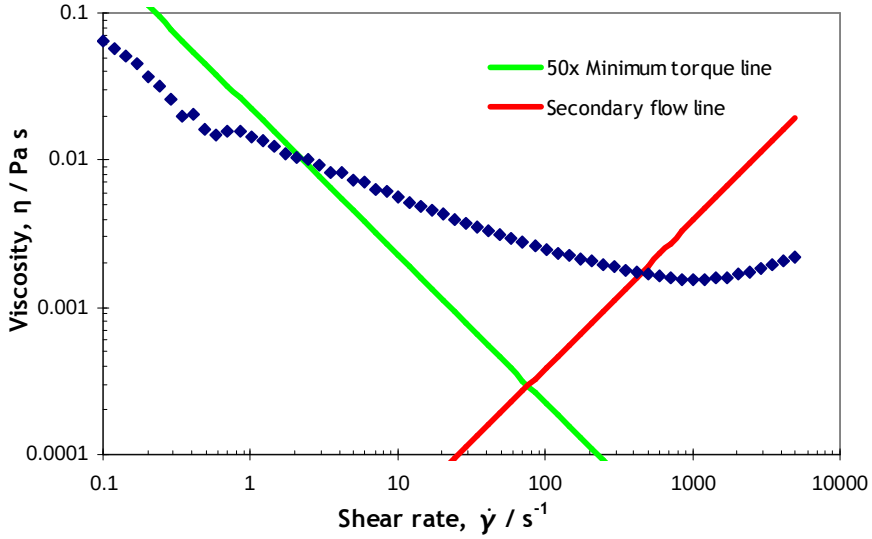

Figure 3.2: Example of a flow curve with the 50x minimum torque line and secondary flow line.

3.3 Results and discussion of shear viscosity measurements

3.3.1 Influence of temperature on shear viscosity

The steady shear viscosity of the two aqueous solutions of PAA, with a concentration of 50 and 125 ppm, were measured. First the influence of temperature is examined and the results are presented in Figure 3.3 a and b. As can be seen in Figure 3.3 the viscosity decreases with increasing temperature. This result is expected since at higher temperatures, molecules possess higher kinetic energy. An increase in kinetic energy results in a faster movement of the molecules, which means less resistance to the flow and therefore lower viscosities. In the literature, there are a vast number of models relating the viscosity of liquids to the temperature (Arrhenius 1887; Williams et al. 1955; Seeton 2006).

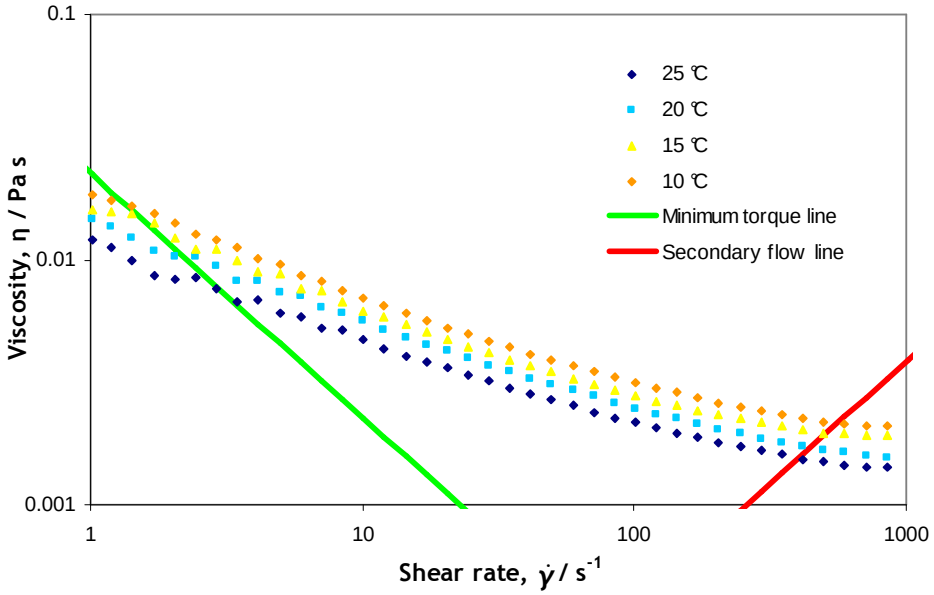

(a) PAA 50 ppm

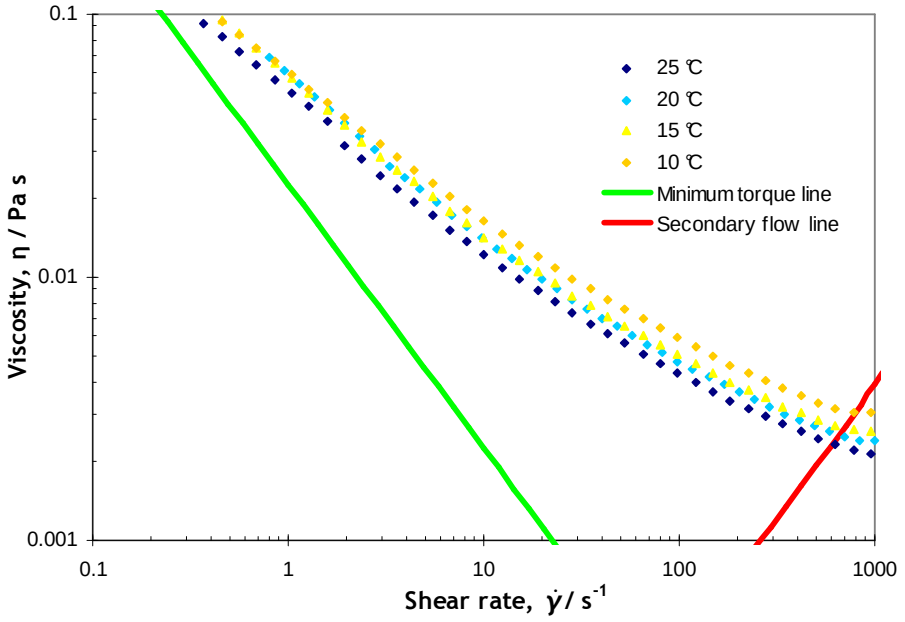

(b) PAA 125 ppm

Figure 3.3: Shear viscosity measurements for PAA 50 ppm (a) and PAA 125 ppm (b) at different temperatures.

Using the time-temperature superposition principle, a master curve was obtained for each fluid at a reference temperature (293K). The corresponding shift factors to make the curves overlap are calculated by:

$$a_T = \frac{\eta(T)}{\eta(T_{ref})}\frac{T_{ref}}{T}\frac{\rho_{ref}}{\rho} \tag{3.5}$$

where a_T is the shift factor, η(T) is the viscosity at temperature T, $\eta(T_{ref})$ and ρ_{ref} are the viscosity and density at the reference temperature T_{ref} respectively. Since for the small range of temperatures used in the measurements the fluid density is approximately constant and the ratio T_{ref}/T is also close to unitary the shift factor simplifies to:

$$a_T = \frac{\eta(T)}{\eta(T_{ref})} \tag{3.6}$$

After the determination of the shift factor the master curve can be determined using:

$$\eta_r = \eta(T_{ref}) = \frac{\eta(T)}{a_T} \tag{3.7}$$

$$\dot{\gamma}_r = \dot{\gamma}(T_{ref}) = a_T\dot{\gamma} \tag{3.8}$$

with η_r the reduced viscosity (Pa s) and $\dot{\gamma}_r$ the reduced shear rate (s^{-1})

The graphs of the master curves for PAA 50ppm and 125ppm are shown in Figure 3.4 a and b, respectively.

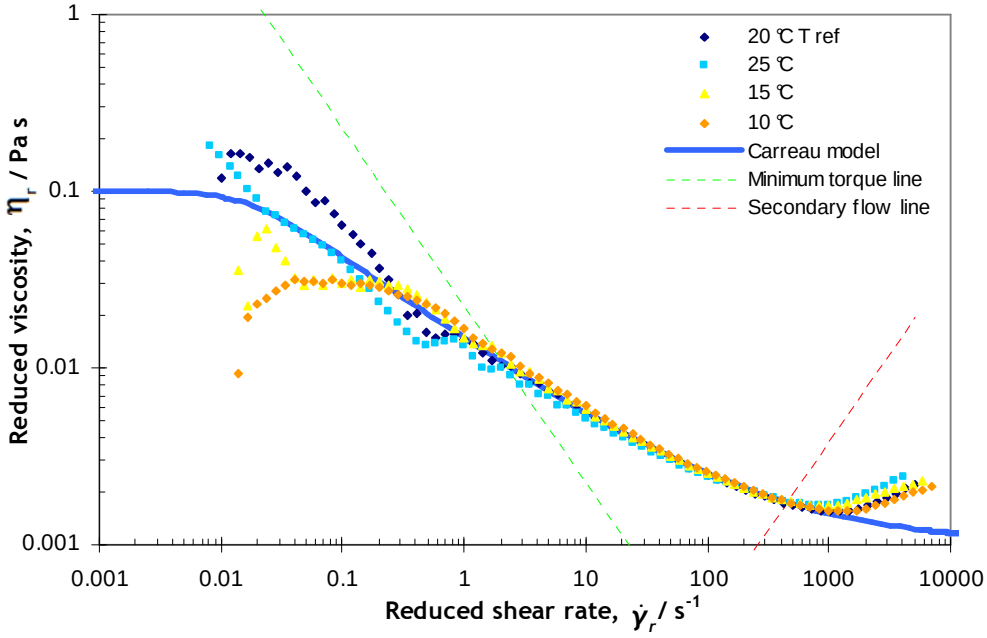

(a) PAA 50 ppm

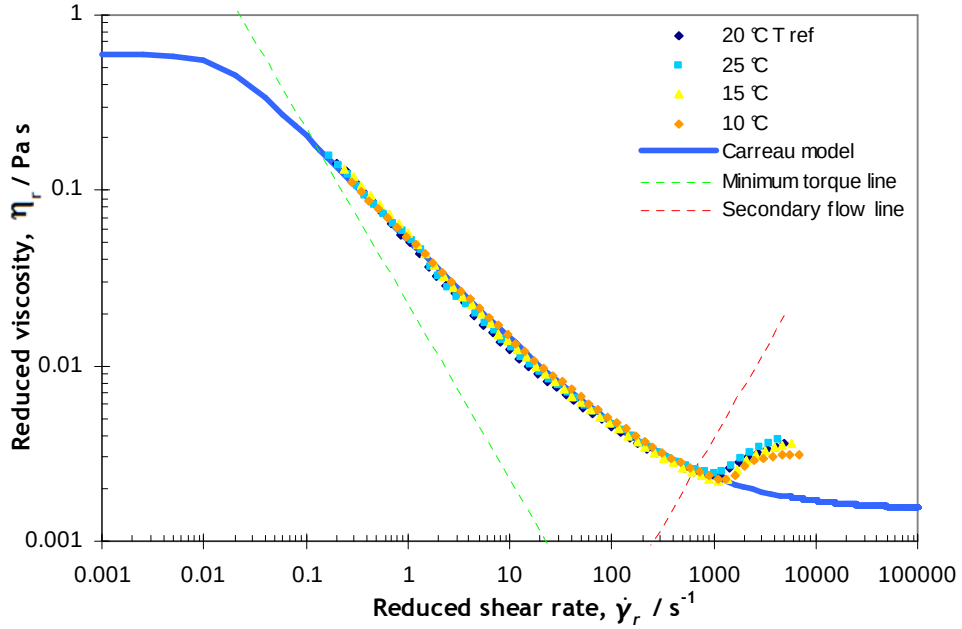

(b) PAA 125 ppm

Figure 3.4: Steady shear viscosity master curves (T_{ref} = 298.15 K) for PAA 50 ppm (a) and 125 ppm (b) with a fit of the Carreau model.

The PAA solutions present a shear thinning behavior which is commonly observed in dilute polymer solutions (Cross 1979; Yang 2000; Ryder and Yeomans 2006). To obtain a relation between the viscosity and shear rate, the Carreau model (Bird and Carreau 1968) was fitted to the experimental master curves. The Carreau model relates the viscosity to the shear rate by the following equation:

$$\eta_c = \eta_\infty + \frac{\eta_0 - \eta_\infty}{\left[1 + \left(\Lambda\dot{\gamma}\right)^2\right]^{\frac{1-n}{2}}} \tag{3.9}$$

in which η_∞ is the viscosity (Pa s) at a infinitely large shear rates, η_0 is the viscosity with a zero shear rate (Pa s), Λ is the specific time at which shear thinning effects will start (s) and n the power law exponent. Fitting this model (Figure 3.4 a and b) to the experimental data yields the parameters presented in Table 3.1.

Table 3.1: Parameters of the Carreau model fit for the 125 and 50 ppm PAA solutions.

Solution	η_∞ (Pa s),	η_0 (Pa s)	Λ (s)	n
PAA 125 ppm	0.0015	0.60	60	0.40
PAA 50 ppm	0.0010	0.10	60	0.52

3.3.2 Influence of amount of surfactant on shear viscosity

Next, the influence of SDS on the viscosity is examined. The results can be seen in Figure 3.6 for the PAA 125 ppm solution. Using a concentration of 0.1% the viscosity decreases almost five times related to the solution without any surfactant. For the 50 ppm solution the same effect was observed. To explain this effect, the concentration of the polymer in the solution should be discussed first.

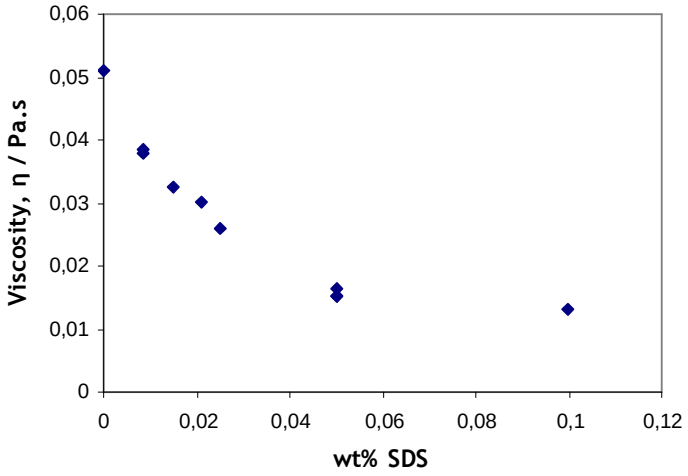

Figure 3.5: Influence of sodium dodecyl sulphate (SDS) concentration on viscosity of PAA125 ppm at $\dot{\gamma}=1.04\ s^{-1}$ *(20°C).*

In highly concentrated polymer solutions, the addition of a low amount of SDS will result in an increase in viscosity. The SDS interacts with the hydrophobic part of the polymer, and micelles will be created. The micelles aggregate with other polymer chains at a critical aggregation concentration (CAC) resulting in crosslinking and a further increase in viscosity (Ma et al. 2002; Penott-Chang et al. 2007). Above this concentration, the viscosity will decrease because the solution will be saturated with micelles. Electrostatic repulsion (SDS is an ionic surfactant) of the micelles will cause a decrease in crosslinking and subsequently a decrease in the viscosity (Figure 3.7).

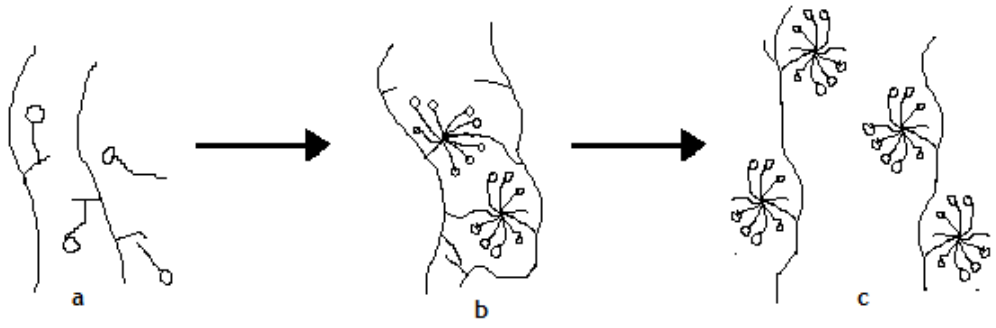

Figure 3.6: Schematic interpretation of the effect of surfactant on the viscosity of a solution with a high polymer concentration. At very low SDS concentrations, the surfactant starts to interact with the polymer side groups (a). At higher concentrations the micelles start to aggregate and crosslinking of the polymer occurs and the viscosity increases (b). If the polymer chains are saturated the polymers will not interact with each other resulting in a decrease in viscosity (c) (Ma et al. 2002; Penott-Chang et al. 2007).

However, the 125 and 50 ppm solutions used here are dilute solutions in which polymer chains behave like they are independent (Scott 2004). Therefore, crosslinking and interchain interactions seem an unlike event. Instead, intrachain interactions and the conformation of the polymer chain need to be analyzed. Hai and Han (2006) studied the viscosity of various concentrations of SDS in 1 wt% PAA solutions. First, they found a decrease in viscosity which can be explained as follows. PAA has an amide group which hydrolyzes in water to form NH_3 and a COO^- group. Due to the repulsive forces of the negative charges, the polymer chains will be stretched. Addition of SDS leads to a reduction of these repulsive forces because it forms complexes around the polymer that result in a contraction of the polymer chain and therefore a lower viscosity. After the decrease in viscosity, a small increase was found at the CAC. This can be due to the extension of the polymer chains by the formation of SDS-PAA complexes. Above the CAC, the solution will become saturated with SDS and free micelles will exist (Figure 3.8). The free micelles and counter-ions will increase the ionic strength of the solution. Electrostatic screening and hydrophobic interactions will lower the viscosity by contraction of the polymer chains.

In this work, only a decrease in viscosity is observed. To determine if the solution is already saturated, the critical aggregate concentration is calculated based on the study of Hai and Han (2006): 0.173 g SDS/g PAA. This excess amount corresponds to $2.16 \cdot 10^{-5}$ g of SDS in one gram of the 125 ppm solution, which translates as weight percentage of $2.16 \cdot 10^{-3}$. In the experiments, the lowest weight percentage used was $8.6 \cdot 10^{-3}$, corresponding to the third stage of Hai and Han's (2006) study and therefore only a decrease in viscosity is observed.

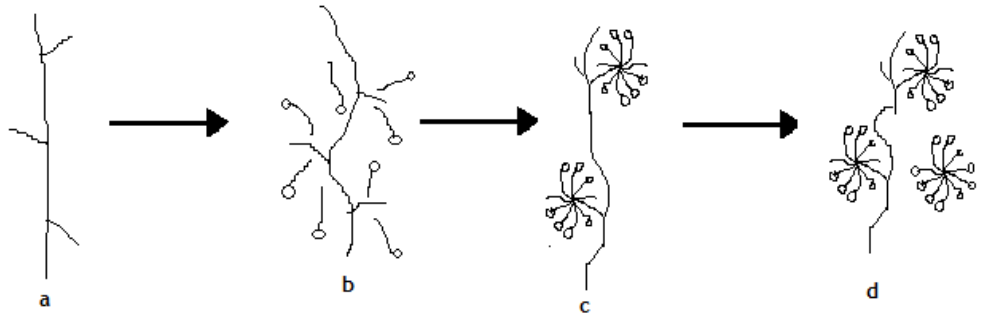

Figure 3.8: Schematic interpertation of the effect of surfactant on the viscosity of a low concentrated polymer solution. First the polymer chains are stretched due to repulsive forces of the hydrolyzed side groups (a), the surfactant interacts with the polymer resulting in decrease of repulsive forces and coiling of the chain (b). At the CAC the viscosity will shortly increase due to the formation of complex PAA-SDS structures. (c). Free micelles and counterions cause an increase in ionic strength and viscosity decreases further (d) (Hai and Han 2006).

3.3.3 Influence of NaCl on viscosity

NaCl is typically added to PAA solutions to make the fluid electrically neutral. The effect on the viscosity is examined and the results for the PAA 125 ppm solution are shown in Figure 3.9. For PAA 50 ppm similar results were obtained but not shown here.

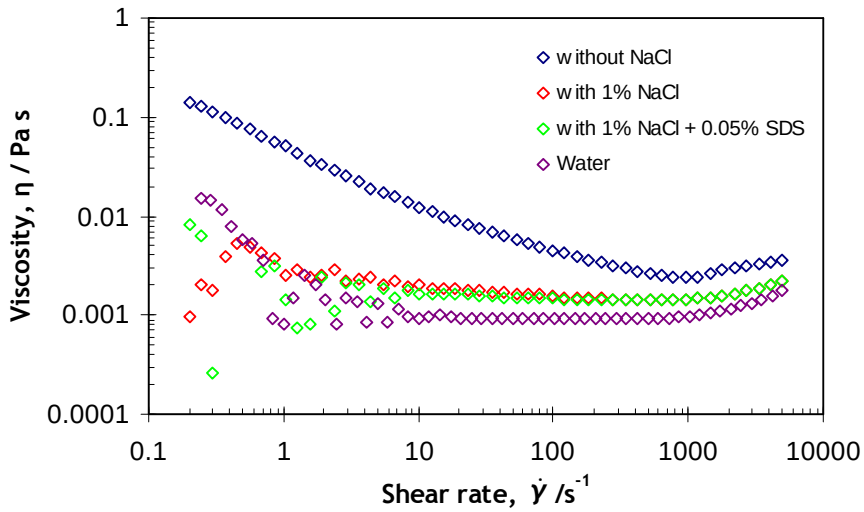

Figure 3.9: Effect of sodium chloride (NaCl) on the shear viscosity of PAA 125 ppm in comparison with water.

With the addition of NaCl, shear thinning effects significantly decrease and the flow curve becomes similar to that of a Newtonian fluid, in this case water. The decrease in viscosity is explained in detail by Ghannam (1998). As explained before, the polymer chains are hydrolyzed in water resulting in a stretched molecule. The addition of NaCl will neutralize the negatively charged carbonyl (COO^-) groups and the repulsive forces will decrease. Therefore the radius of giration of the polymer chain will decrease resulting in a lower viscosity.

Adding 0.05% SDS to the PAA 125 ppm solution with 1% sodium chloride does not significantly decrease the viscosity. This is because the polymer chains are already coiled so the surfactant will have less effect.

The Newtonian-like behavior of the shear viscosity may suggest the fluid is not elastic. However, measurements of the relaxation time (cf. Section 3.4.2) show that the PAA solutions with NaCl are still elastic. This means that the addition of sodium chloride confers to the PAA solutions a behavior similar to that of a Boger fluid, in which the viscosity is independent of shear rate but still exhibits elasticity (Boger 1977). However, a major

difference is that in this case the viscosities are lower than those typically found for Boger fluids, which are prepared by adding a high viscosity solvent.

3.4 Extensional rheology

3.4.1 Experimental Technique

A capillary break-up extensional rheometer (Haake CaBER 1, Thermo Scientific) is used to measure the relaxation time. In the apparatus there are two plates (R_0 = 3mm), one is stationary and the other can move up and down. In the initial state the plates are separated by a gap h_0 and a sample of fluid is loaded between the plates as shown in Figure 3.10 a. Next, the top plate moves very fast upwards (50 ms) to a final height (h_f), originating a cylindrical thinning fluid filament in the central region between the two plates (cf. Figure 3.10 b). The diameter of this filament is measured by a laser as a function of time. It is important that the diameter of the cylindrical filament is measured without the interference of small droplets (Scott 2004). Therefore the initial height and final height need to be chosen adequately. An initial height of 3 mm is chosen and a final height of 12 mm based on preliminary tests.

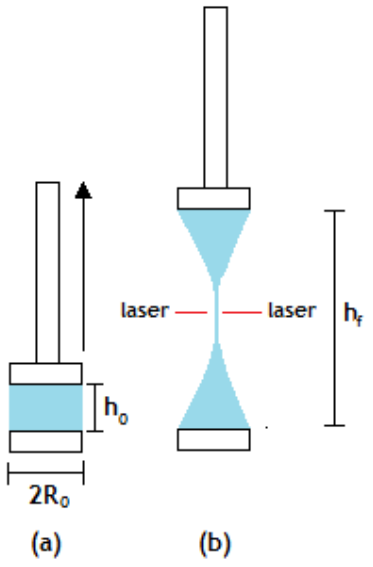

Figure 3.10: Caber measurements. A fluid sample is put between the plates (a). The upper plate moves while the laser measures the filament diameter as function of time (b).

For viscoelastic fluids, a stress balance between surface tension and elastic stresses results in an exponential decay in the filament radius (R_f) with time (Entov and Hinch 1997):

$$\frac{R_f}{R_0} = C\, exp\left(\frac{-t}{3\lambda}\right) \tag{3.10}$$

with R_0 (m) is the radius at time t = 0, C is a fluid dependant constant and λ is the relaxation time (s).

The relaxation time can be easily obtained by plotting the logarithm of the R_f/R_0 as a function of time and fitting the linear form of Equation 3.9 to the linear part of the measured curve. The slope obtained will be equal to $-1/3\lambda$.

3.4.2 CaBER results

CaBER tests were performed to determine the relaxation time for each fluid. Additionally each test is performed several times to assess the repeatability (not shown here), which was shown to be satisfactory. The results for the four fluids used throughout the experiments are shown in Figure 3.11. The top plate reaches the final height at t_0 = 0.05 s

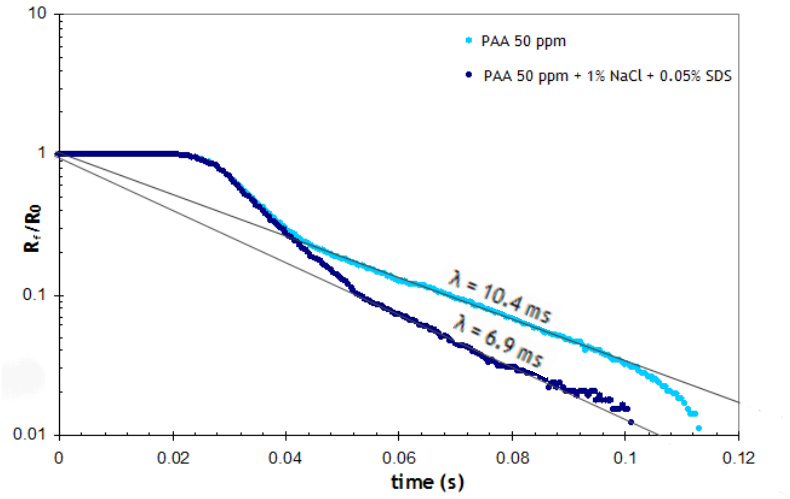

a) PAA 50 ppm

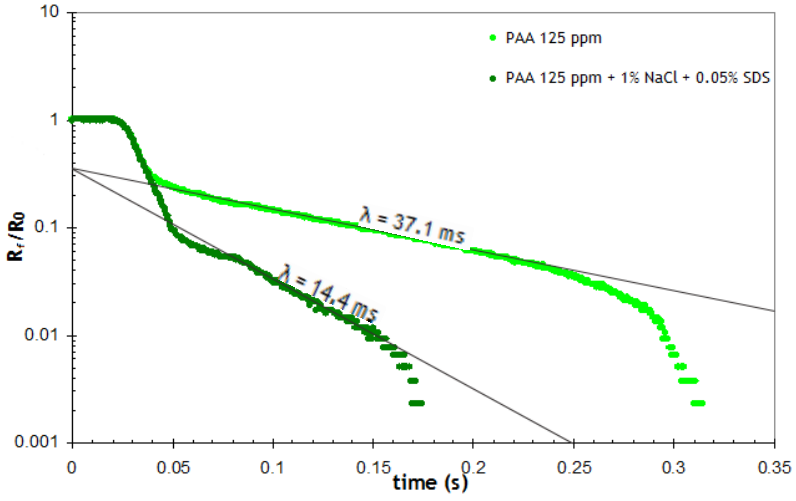

b) PAA 125 ppm

Figure 3.11: Evolution of the filament radius as a function of time during a CaBER experiment for PAA 50 ppm with and without additives (a) and PAA 125 ppm with and without additives (b).

Relaxation times are obtained by fitting the data with an elastic model in which the filament radius decreases exponential with time as explained in section 3.4.1. This fit resulted in the relaxation times presented in Table 3.2.

Table 3.2: Relaxation times of the fluids used in the experiments.

Fluid	λ (ms)
PAA 125 ppm	37.1
PAA125 ppm +1% NaCl + 0.05% SDS	14.4
PAA 50 ppm	10.4
PAA 50 ppm + 1% NaCl + 0.05%SDS	6.9

The relaxation time decreases with decreasing concentration as expected. Furthermore, the relaxation time decreases by inclusion of the additives. Since sodium chloride causes coiling of the polymer strings, the extended state correspondents to a chain with a smaller radius of gyration than without additives. Therefore the time to go from extended to relaxed state will be shorter and so the relaxation time is expected to decrease.

3.5 Summary of fluid characterization

In Table 3.3 the properties of the fluids used in the experiments are summarized. These include PAA solutions with concentrations 50 and 125 ppm without and with additives (1% NaCl + 0.05% SDS), which were found out to significantly change the rheological properties of the fluids.

Table 3.3: Summary of fluid properties used throughout experiments at 20°C.

Fluid	η (mPa s)	λ (ms)	ρ (kg/m^3)*
Water	1.00	-	998.0
PAA 125 ppm	Carreau model (Table 3.1)	37.1	998.2
PAA 125 ppm + 1% NaCl +0.05% SDS (PAA 125 ppm +)	1.44	14.4	1005.1
PAA 50 ppm	Carreau model (Table 3.1)	10.4	998.0
PAA 50 ppm + 1% NaCl + 0.05% SDS (PAA 50 ppm+)	1.17	6.9	1004.9

* measured with a 25 ml picnometer

4 Flow characterization

4.1 Microchannel fabrication

Since rapid manufacturing is preferred soft lithography is chosen as method to fabricate the planar microchannels. The SU-8 mold was already available, and was manufactured at the KNI foundry (http://www.kni.caltech.edu) at the California Institute of Technology. First, a few drops of tridecofluoro-1,1,2,2-tetrahydrooctyl-1-trichlorosilane (United Chemical Technologies) are put on a petri dish with the mold, to silanize the mold for 20 minutes. Two solutions of PDMS and curing agent (Dow Corning:Sylgard 184) are prepared with ratios of 5:1 and 20:1. A vortex mixer is used to homogenize the solutions. In order to remove the air bubbles that appear during the mixing procedure, the solutions are degassed for several minutes using a vacuum pump. Next, the silanized mold is covered with the 5:1 polymer solution and degassed with a vacuum pump. Remaining air bubbles are removed by pricking with a thin wire. After filling the molds they are put in the oven to cure the PDMS for 20 minutes at 80°C. Simultaneously, glass slides are cleaned and spincoated with the 20:1 solution of PDMS and curing agent onto the glass slides for 50 seconds in a spin coater (Laurell WS-650S-6NPP). The glass slides and the molds covered with PDMS are then put in the oven to cure the PDMS for 20 minutes at 80°C. After curing, the PDMS layer with microchannels is cut out from the mold. Inlet, outlet and pressure ports are made into the channels using a small syringe tip. Finally, the microchannels can be sealed with the glass slide and put into the oven for approximately 24 hours at 80°C to promote a better adhesion.

4.2 Microchannel geometry

Microchannel geometries with symmetric and asymmetric contraction/expansions are used. These two geometries are chosen in order to have two different simplified one-dimensional models of a porous medium, as sketched in Figure 4.1. The spheres illustrated represent the particles in an isotropic porous medium.

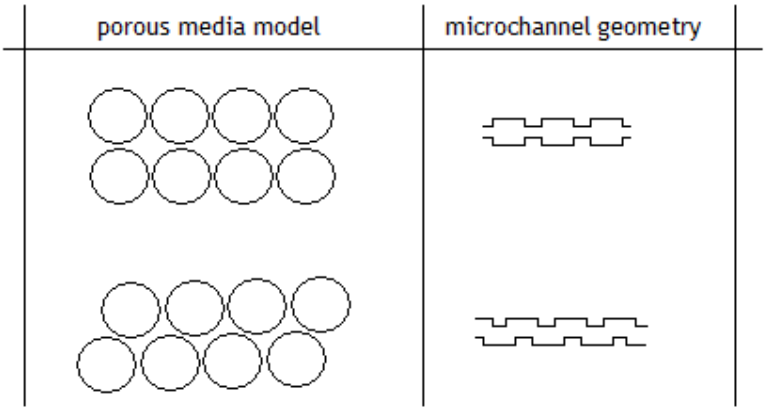

Figure 4.1: Porous medium model with corresponding microchannel geometry analogue.

The dimensions of the microchannels used are presented in Table 4.1, with the primary dimensions defined in Figure 4.2.

Table 4.1: Dimensions of used microchannels.

Dimensions	Asymmetric	Symmetric
W_1	100 µm	100 µm
W_c	66 µm	33 µm
H	100 µm	100 µm
L_1	100 µm	33 µm
L_2	100 µm	33 µm

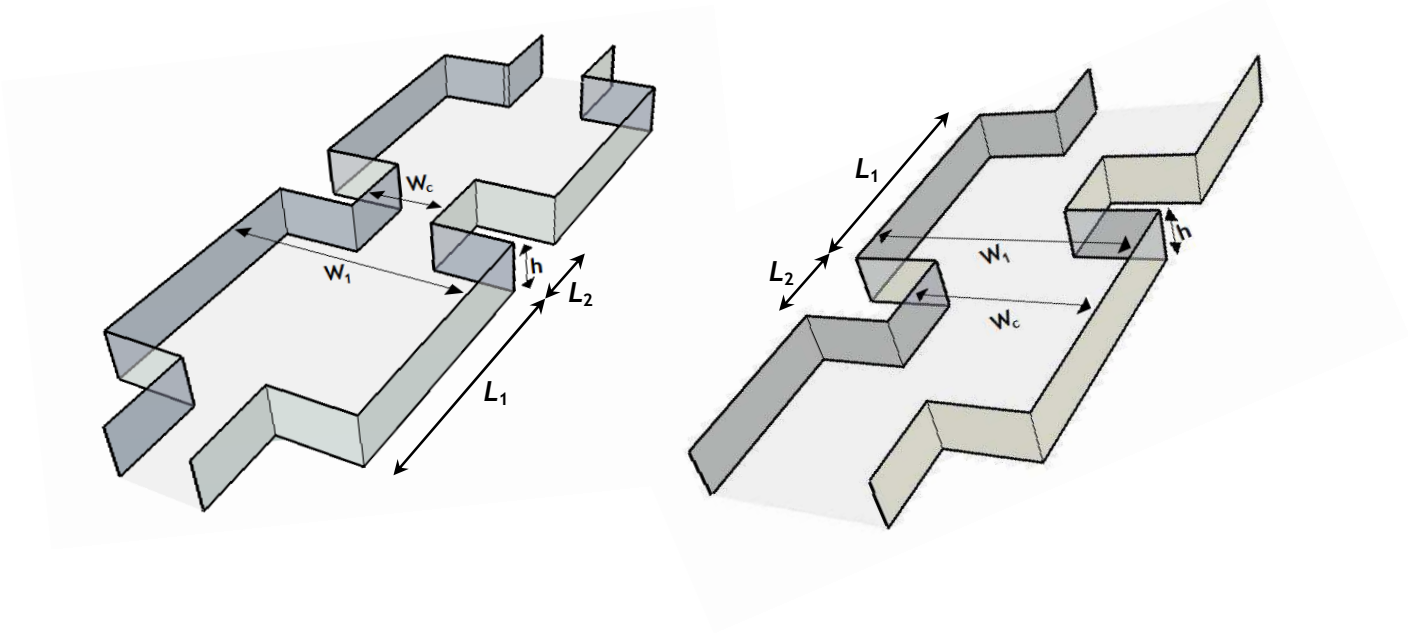

Figure 4.2: Symmetric and asymmetric channels used and definition of some geometrical variables.

4.3 Visualizations

In order to understand the flow patterns, visualizations are carried out using a fluorescence inverted microscope (Leica DMI 5000M) coupled with a 10x objective (NA=0.25). Therefore the fluid is seeded with tracer particles 1 μm in diameter (Nile Red, Molecular Probes, Invitrogen, Ex/Em: 520/580 nm). Streak line images were obtained at different flow rates using a 100 W mercury lamp as illumination source and using long exposure times. In Figure 4.3 the experimental set up is shown. Visualizations are done with water with 0.05% SDS (Sigma Aldrich) and polyacrylamide aqueous solutions with 1 wt% NaCl and 0.05% SDS. Symmetric and asymmetric contraction/expansion geometries are used, as illustrated in Figure 4.2.

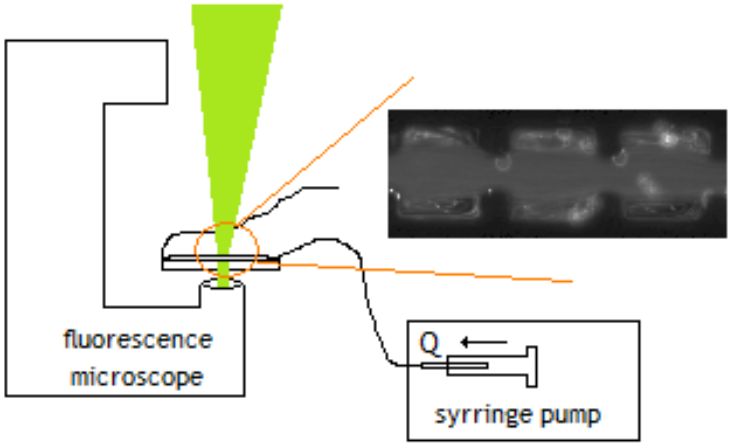

Figure 4.3: Experimental set up visualizations.

4.4 Pressure drop measurements

Pressure drop measurements were carried out for varying flow rates, using differential pressure sensors (Honeywell 26PC) which can cover a differential pressure range of ±3.5kPa, ±6.9kPa and ±34.9kPa. In Figure 4.4 the experimental set up is showed.

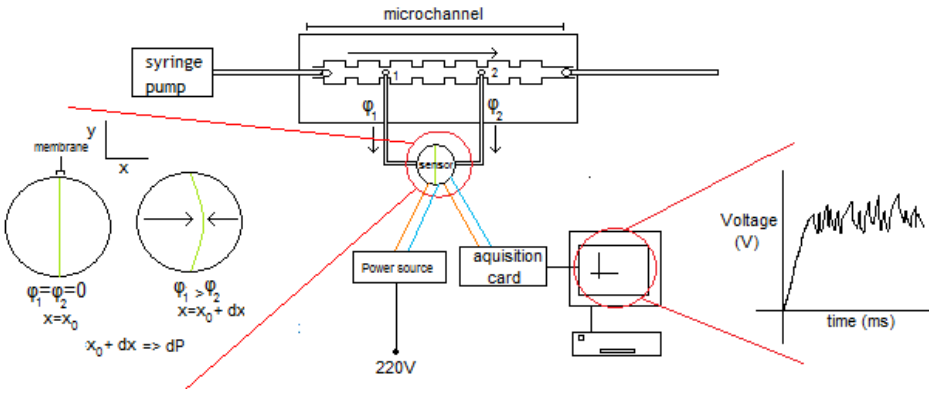

Figure 4.4: Experimental set up pressure drop measurements.

First, the signal with no flow ($Q = 0$) is obtained. Afterwards, a flow rate is imposed using a syringe pump (Nemesys, Cetoni) and the measurement is carried out for a certain time until steady-state conditions are achieved. Then, the measured voltage data is converted to pressure drop data using the correct calibration. Since there are some fluctuations in the measured signal, the average signal is considered for steady flow conditions, as illustrated by the red points in Figure 4.5. Depending on the flow rate and corresponding pressure drop the pressure sensor was chosen. At low flow rates a pressure sensor with a small range was used in order to get more accurate results.

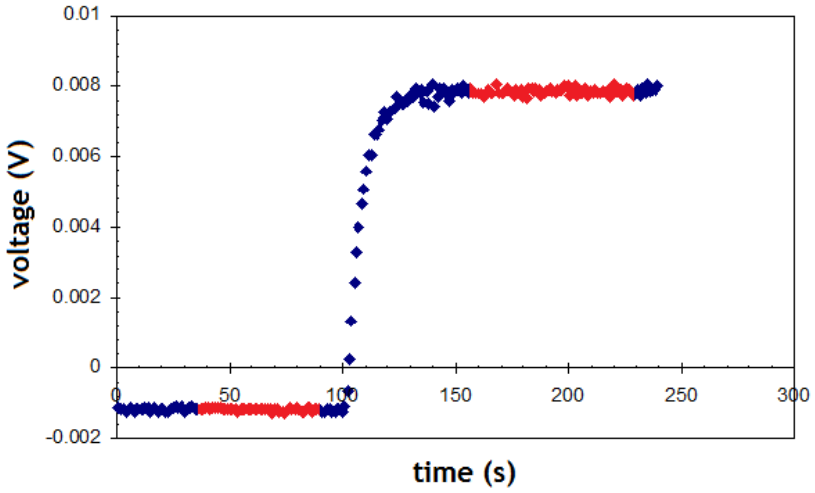

Figure 4.5: Illustration of a pressure drop measurement. At $t \approx 100$ a constant flow rate is imposed. The average value is determined from the signals in the red domain.

4.5 Repeatability

In the visualizations several pictures at the same flow rate are taken. In pressure drop measurements the trend determined if a point should be measured again. If a too high pressure drop is measured, comparing with the trend of previously measured data, this could indicate that air bubbles or small pieces of PDMS were present in the channel partially blocking it. Visual inspection of the channel is done when this happens, and corrective actions are undertaken, namely unblocking the channel by imposing a large flow rate, or when necessary changing the working channel.

4.6 Dimensionless numbers

Three dimensionless numbers are defined here to characterize the flow. The Reynolds number, which represents the ratio between inertial and viscous forces, is defined as:

$$Re = \frac{\rho v_c W_c}{\eta(\dot{\gamma})} \tag{4.1}$$

where ρ is the density (kg/m^3), v_c the average velocity (m/s) in the narrow region of the channel (with width W_c) contraction, and $\eta(\dot{\gamma})$ is the shear viscosity (Pa s) which is a function of the shear rate, $\dot{\gamma}$ (s^{-1}) which can be estimated as:

$$\dot{\gamma} = \frac{2v_c}{W_c} \tag{4.2}$$

For the shear thinning fluids the viscosity is a function of shear rate with the Carreau model according to Eq. 3.9 in Section 3.3.1).

For the constant viscosity viscoelastic fluids (usually known as Boger fluids) the shear viscosity is calculated as an average over the measured range.

The Deborah number is used to see the importance of elastic effects comparing to the specific timescale of the system. The Deborah number is here defined as:

$$De = \dot{\gamma}\lambda = \frac{2\lambda v_c}{W_c} \tag{4.3}$$

where λ represents the relaxation time of the fluid (s).

The elasticity number is also used and is defined by the ratio between *De* and *Re*:

$$El = \frac{De}{Re} = \frac{2\lambda\eta}{\rho W_c^2} \tag{4.4}$$

Since the viscosity is nearly constant in the fluids with additives, the elasticity number is in these cases independent of kinematics.

4.7 Results

The results of the visualizations are presented in Figures 4.6-4.10 for the asymmetric channel and in Figures 4.12-4.16 for the symmetric channel. While the pressure drop measurements are presented in Figures 4.11 and 4.17. In all the pictures shown, the flow direction is from left to right.

4.7.1 Asymmetric channel

Deionized water + 0.05% SDS (*El*=0)

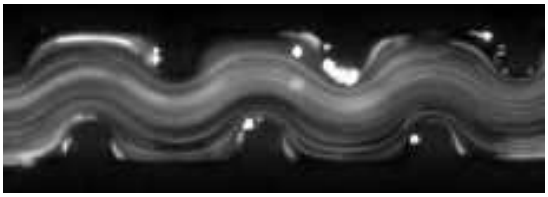

Q=0.1 ml/hr Re =0.27 (very small Mofatt vortices)

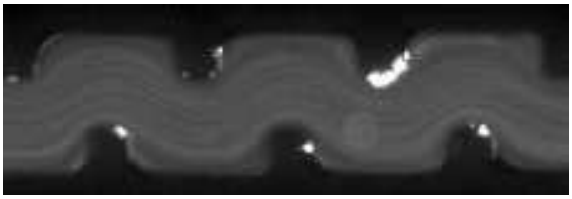

Q=5.0 ml/hr Re =13.7 (very small Mofatt vortices)

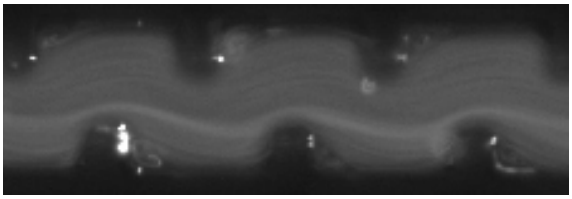

Q=9.0 ml/hr Re=24.65 (corner vortices downstream of the expansion)

Figure 4.6: Visualization of flow patterns in an asymmetric channel of deionized water with 0.05% SDS, for various flow rates.

PAA 50 ppm without additives

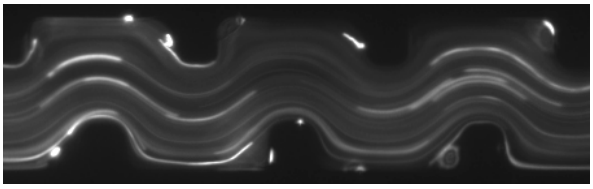

Q = 0.1 ml/hr Re = 0.128 De = 1.31 El = 10.2

(small Mofatt vortices)

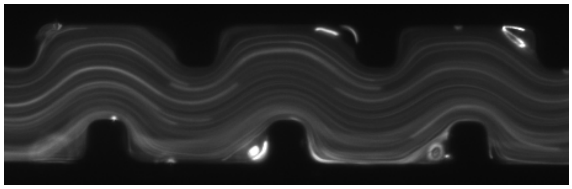

Q = 0.3 ml/hr Re = 0.452 De = 3.93 El = 8.69

(growing vortices upstream of the contraction)

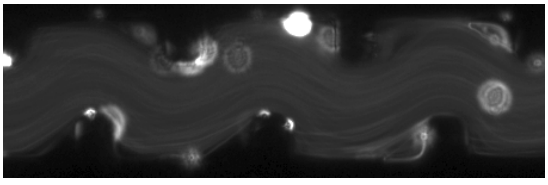

Q = 0.8 ml/hr Re = 1.315 De = 10.5 El = 7.97 (growing vortices upstream of the contraction)

Figure 4.7: Visualization of flow patterns in an asymmetric channel of the PAA 50 ppm solution without additives, for various flow rates.

PAA 50 ppm + 1% NaCl + 0.05% SDS (*El*=3.69)

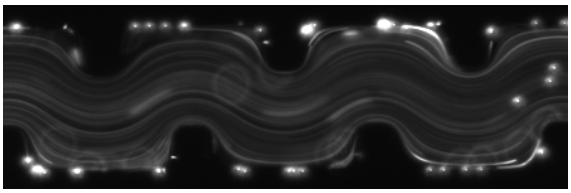

Q=0.1 ml/hr Re=0.239 De=0.880

(small Mofatt vortices)

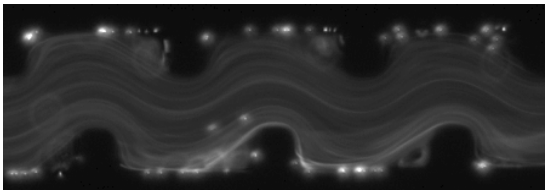

Q=0.4 ml/hr Re=0.954 De=3.53

(small vortices upstream of the contraction)

Figure 4.8: Visualization of flow patterns in an asymmetric channel of the PAA 50 ppm solution with 0.05% SDS and 1% NaCl, for various flow rates.

PAA 125 ppm without additives

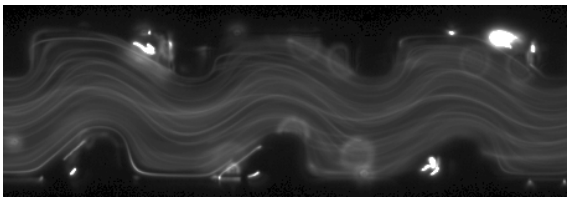

Q=0.1 ml/hr Re=0.0635 De=4.73 El=74.4

(small vortices upstream of the contraction)

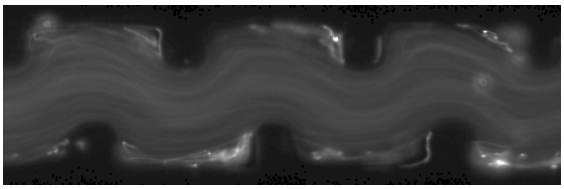

Q=0.7 *ml/hr* Re=0.812 De=33.1 El=40.8

(growing vortices upstream of the contraction and downstream of the expansion)

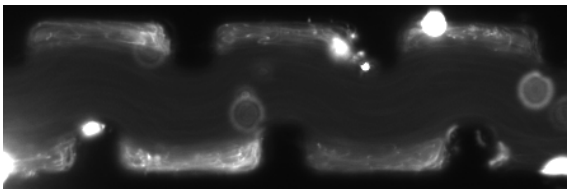

Q=3.0 ml/hr *Re=4.44 De=141.9 El=31.9 (merging vortices)*

Figure 4.9: Visualization of flow patterns in an asymmetric channel *of the PAA 125 ppm solution at various flow rates.*

PAA 125 ppm + 1% NaCl + 0.05% SDS (*El*=9.37)

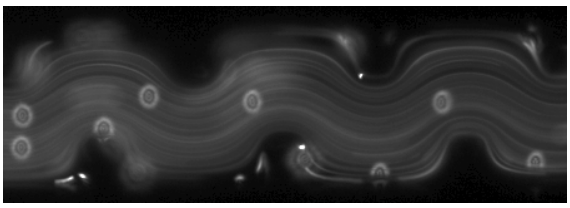

Q = 0.1 ml/hr Re = 0.194 De = 1.82
(no vortices)

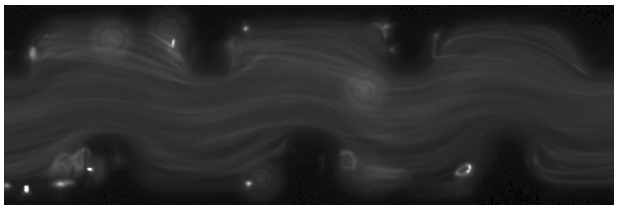

Q = 0.3 ml/hr Re = 0.581 De = 5.45
(small vortices upstream of the contraction)

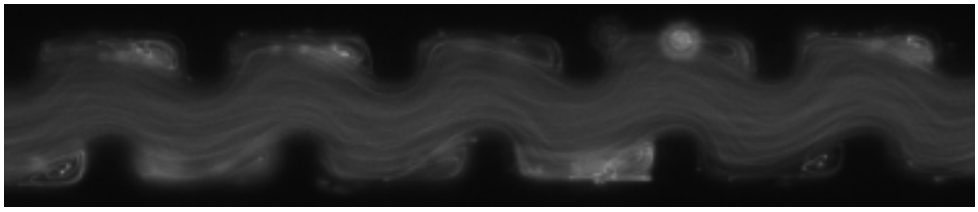

Q = 2.0 ml/hr Re = 3.88 De = 36.4

(growing vortices upstream of the contraction and downstream of the expansion)

Figure 4.10: Visualization of flow patterns in an asymmetric channel of the PAA 125 ppm solution with 0.05% SDS and 1% NaCl, for various flow rates.

The pressure drop measurements obtained with the solutions analyzed are presented in Figure 4.11.

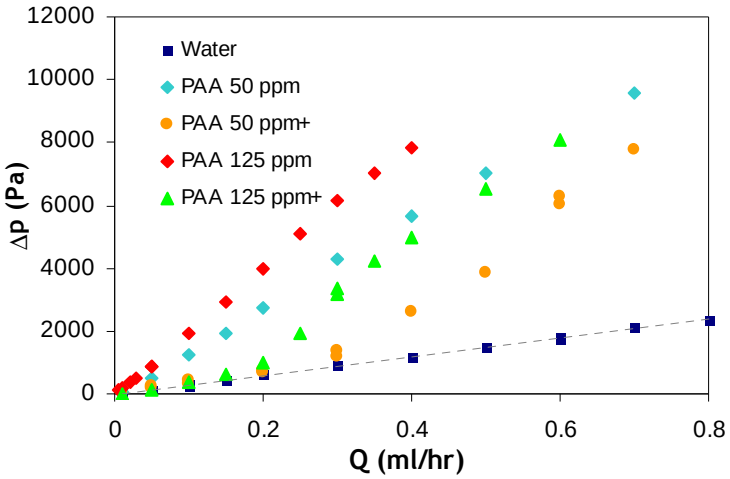

Figure 4.11: Pressure drop measurements for several solutions in the asymmetric microchannels.

4.7.2 Symmetric channel

Deionized water + 0.05% SDS (El=0)

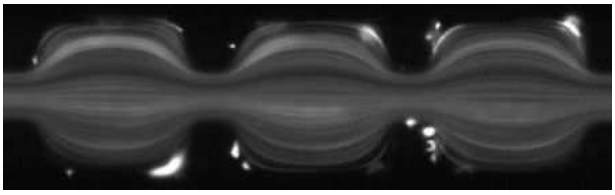

Q = 0.1 ml/hr Re = 0.274

(very small Mofatt vortices)

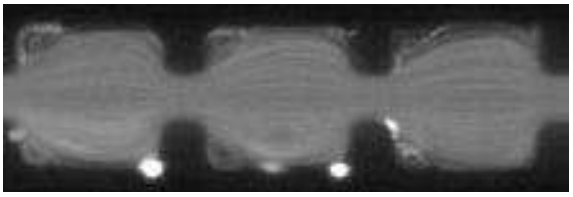

Q = 5.0 ml/hr Re = 13.7 (growing vortices downstream of the expansion and reducing vortices upstream of the contraction)

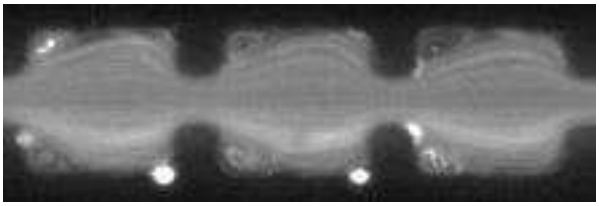

Q = 7.0 ml/hr Re = 19.17 (vortices downstream of the expansion)

Figure 4.12: Visualization of flow patterns in a symmetric channel of deionized water with 0.05% SDS, for various flow rates.

PAA 50 ppm without additives

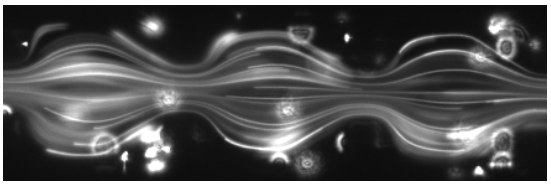

Q = 0.01 ml/hr Re = 0.010 De = 0.52 El = 50.7

(small vortices upstream of the contraction)

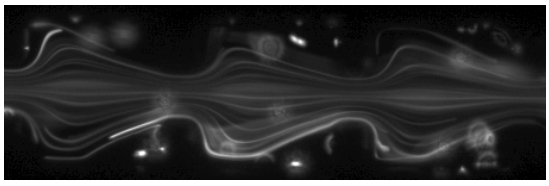

Q = 0.1 ml/hr Re = 0.103 De = 5.24 El = 33.7

(growing vortices upstream of the contraction)

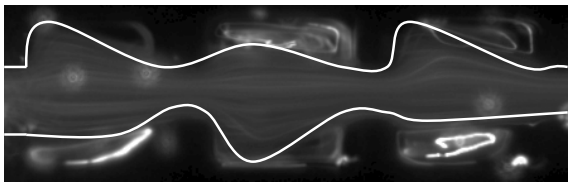

Q = 0.3 ml/hr Re = 0.505 De = 15.7 El = 31.1 (asymmetric flow)

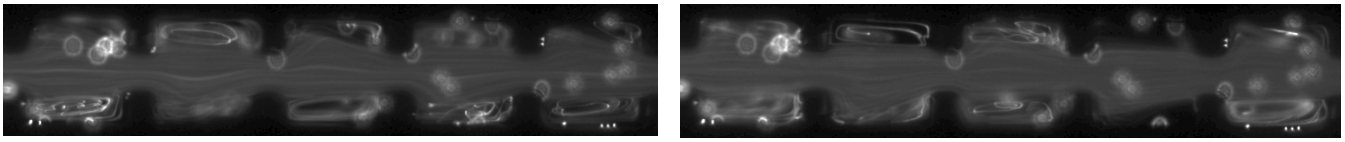

Q = 0.8 ml/hr Re = 1.403 De = 41.9 El = 29.9 (unstable flow)

Figure 4.13: Visualization of flow patterns in a symmetric channel of the PAA 50 ppm solution without additives, for various flow rates.

PAA 50 ppm + 1% NaCl + 0.05% SDS (El=14.79)

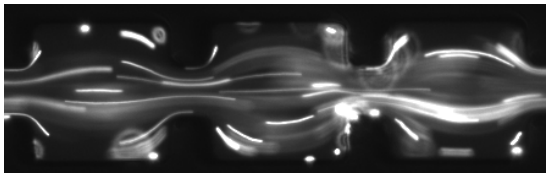

Q = 0.01 ml/hr Re = 0.023 D e= 0.35

(very small Mofatt vortices)

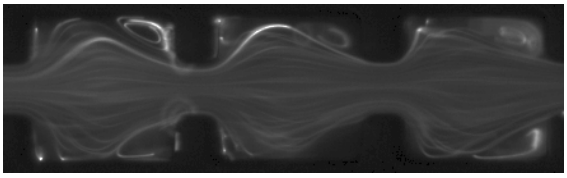

Q = 0.3 ml/hr Re = 0.716 De = 10.6

(growing vortices upstream of the contraction)

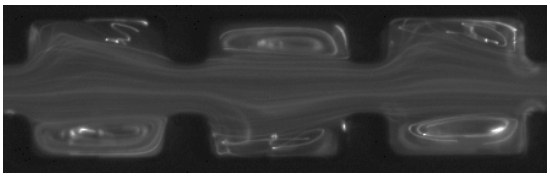

Q = 0.7 ml/hr Re = 1.67 De = 24.7 (asymmetric flow)

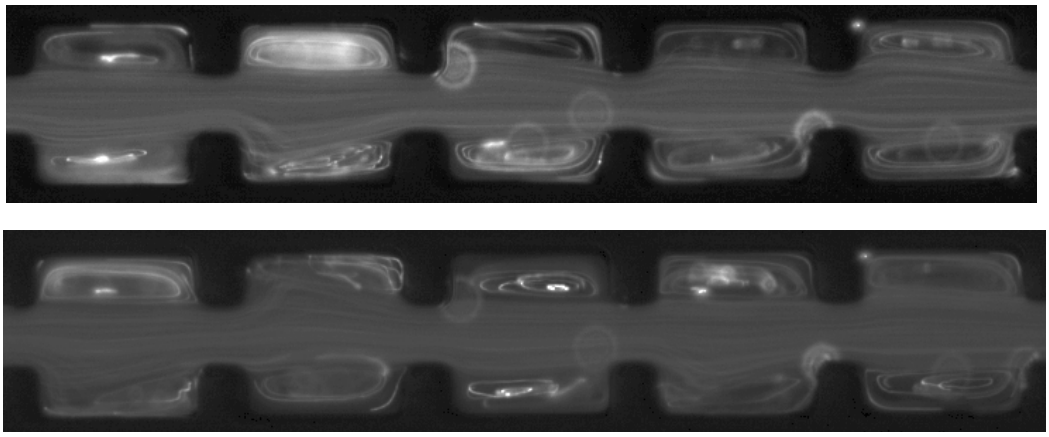

Q = 1.5 ml/hr Re = 3.58 De = 52.92 (unstable flow)

Figure 4.14: Visualization of flow patterns in a symmetric channel of the PAA 50 ppm solution with 0.05% SDS and 1%NaCl, for various flow rates.

.

PAA 125 ppm without additives

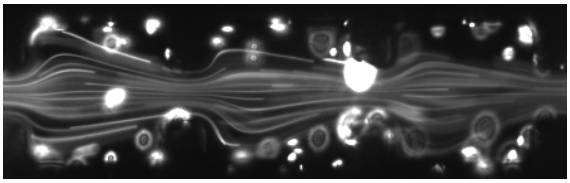

Q = 0.01 ml/hr Re = 0.004 De =1.89 El=440.6

(vortices upstream of the contraction)

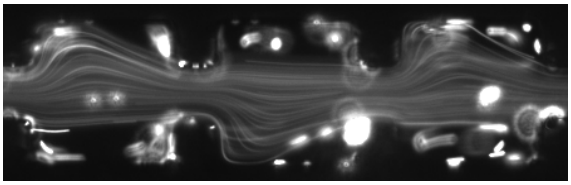

Q = 0.05 ml/hr Re=0.041 De=9.46 El=231.2

(asymmetric flow)

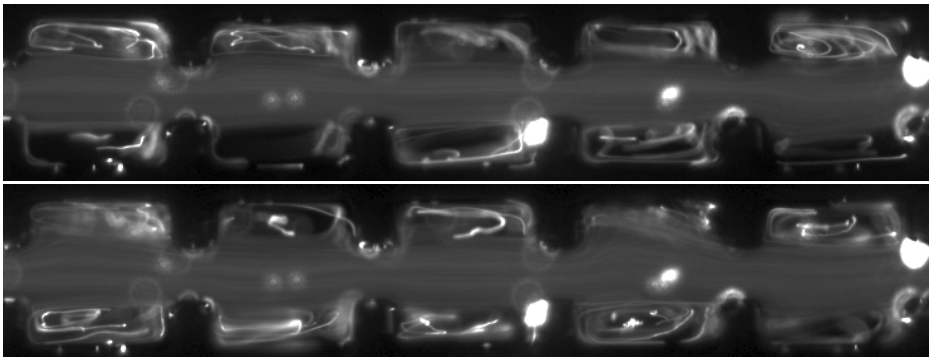

Q=0.8 ml/hr Re=1.194 De=151.4 El=126.8 (unstable flow)

Figure 4.15: Visualization of flow patterns in a symmetric channel of the PAA 125 ppm solution without additives, for various flow rates.

PAA 125 ppm + 1% NaCl + 0.05% SDS (El=36.45)

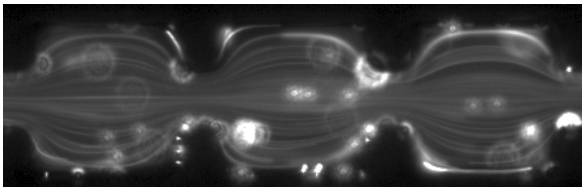

Q = 0.1 ml/hr Re = 0.199 De = 7.27

(small vortices upstream of the contraction)

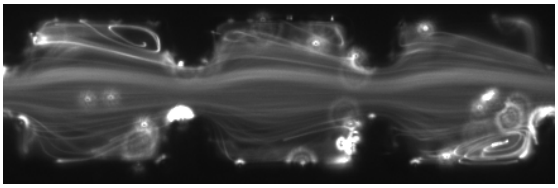

Q = 0.2 ml/hr Re = 0.399 De = 14.5

(growing vortices upstream of the contraction)

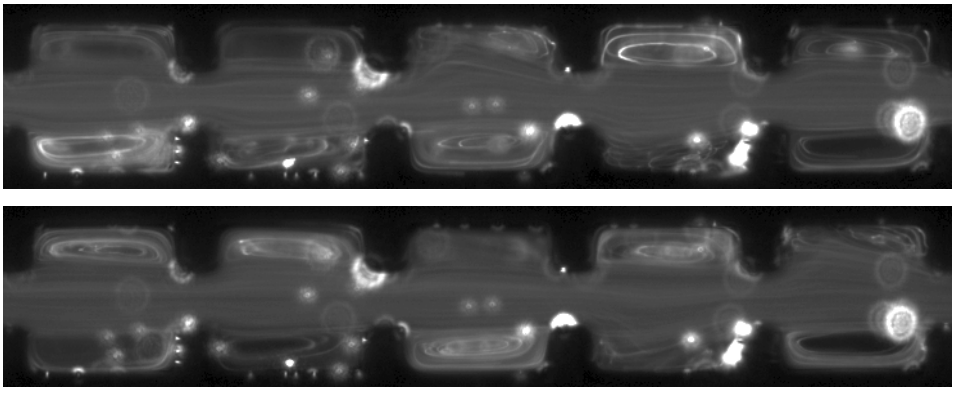

Q = 0.8 ml/hr Re = 1.595 De = 58.2 *(unstable flow)*

Figure 4.16: Visualization of flow patterns in a symmetric channel of the PAA 125 ppm solution without additives, for various flow rates.

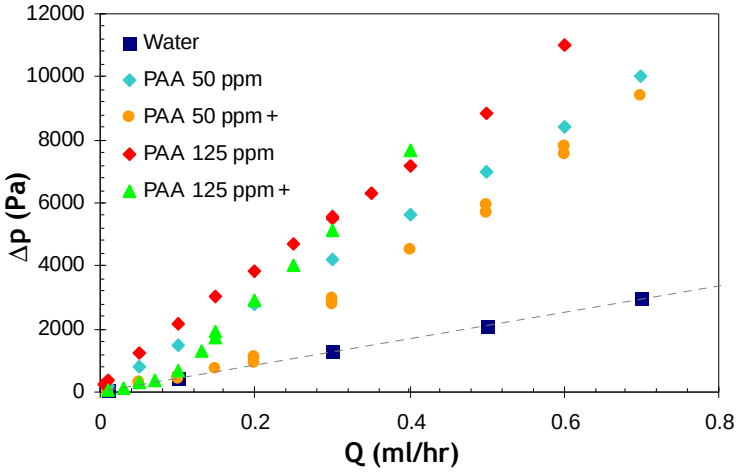

Figure 4.17: Pressure drop measurements for several solutions in symmetric microchannels.

4.8 Discussion

By analyzing the pressure drop data and visualizations, the influence of geometry, additives, polymer concentration are examined. Furthermore the visualizations are analyzed and different flow patterns are observed.

4.8.1 Influence of type of geometry

In pressure drop measurements (Figures 4.11 and 4.17) the same effects for the symmetric and asymmetric channel (117 repeating units both) drop are observed. The critical flow rate, at which a significant increase in the pressure drop is observed, is lower in the symmetric channel than in the asymmetric channel. This can be explained by the fact that the symmetric channel has a more sudden and smaller contraction leading to a stronger extensional flow.

4.8.2 Influence of additives

In the flow visualizations it can be seen that at a critical flow rate elastic effects become important, with the onset of recirculations in the channel cavities. These recirculations are not a consequence of inertia, since they appear at low *Re*. In Table 4.2 the critical flowrates are shown.

By comparing the pressure drop data with the visualizations, a distinction between fluids without additives and with additives needs to be made. For the viscoelastic fluids without additives, the onset of vortices does not correlate to a sudden increase in the pressure drop,

which follows a quasi-linear variation in the whole range of flow rates. With additives the onset of vortices, showed in visualizations, corresponds to a sudden increase in pressure drop. To explain this effect, two ranges of flow rates and the difference in viscous behavior of both fluids needs to be analyzed. Below the critical flow rate, all fluids show a linear variation of pressure drop with flow rate. The fluids without additives (PAA 125 ppm and PAA 50 ppm) show a higher pressure drop due to a higher viscosity. Fluids with additives (PAA 125 ppm + and PAA 50 ppm +) show a variation of pressure drop with the flow rate which is similar to that of water. This is in agreement with the viscosities since they are very similar too. At higher flow rates the absence or presence of an increase in pressure drop can be explained by the viscous behavior of both fluids. The fluids without additives have a shear thinning behavior which leads to a lower viscosity at higher flow rates. This viscous behavior will lead to a lower pressure drop while the elastic behavior originates an increase in pressure drop. These two behaviors apparently compensate, leading to a quasi-linear relation of pressure drop with flow rate for the whole range studied. The viscosity of the fluids with additives is nearly independent of shear rate, therefore the elasticity influence is isolated and is found to originate an increase in pressure drop, as reported in earlier works of viscoelastic fluid flow in porous media (Marshall and Metzner, 1967).

Table 4.2: Critical flow rate for used fluids for symmetric and asymmetric channel.

	Symmetric	**Asymmetric**
PAA 50 ppm	± 0.1 ml/hr	± 0.3 ml/hr
PAA 50 ppm +	± 0.3 ml/hr	± 0.4 ml/hr
PAA 125 ppm	± 0.01 ml/hr*	± 0.1 ml/hr
PAA 125 ppm +	± 0.2 ml/hr	± 0.3 ml/hr

* lowest applied flow rate

4.8.3 Effect of polymer concentration

The effect of polymer concentration is in agreement with what was expected. At higher concentrations a higher increase of pressure drop is observed, due to a higher viscosity (and elasticity) of the fluid.

4.8.4 Flow patterns

The captured images of the visualizations were analyzed and different flow patterns were identified. In the asymmetric channel the flow patterns are similar for all fluids but in the symmetric channel a diverse range of flow patterns was observed and plotted in a *De-Re* map as shown in Figure 4.18.

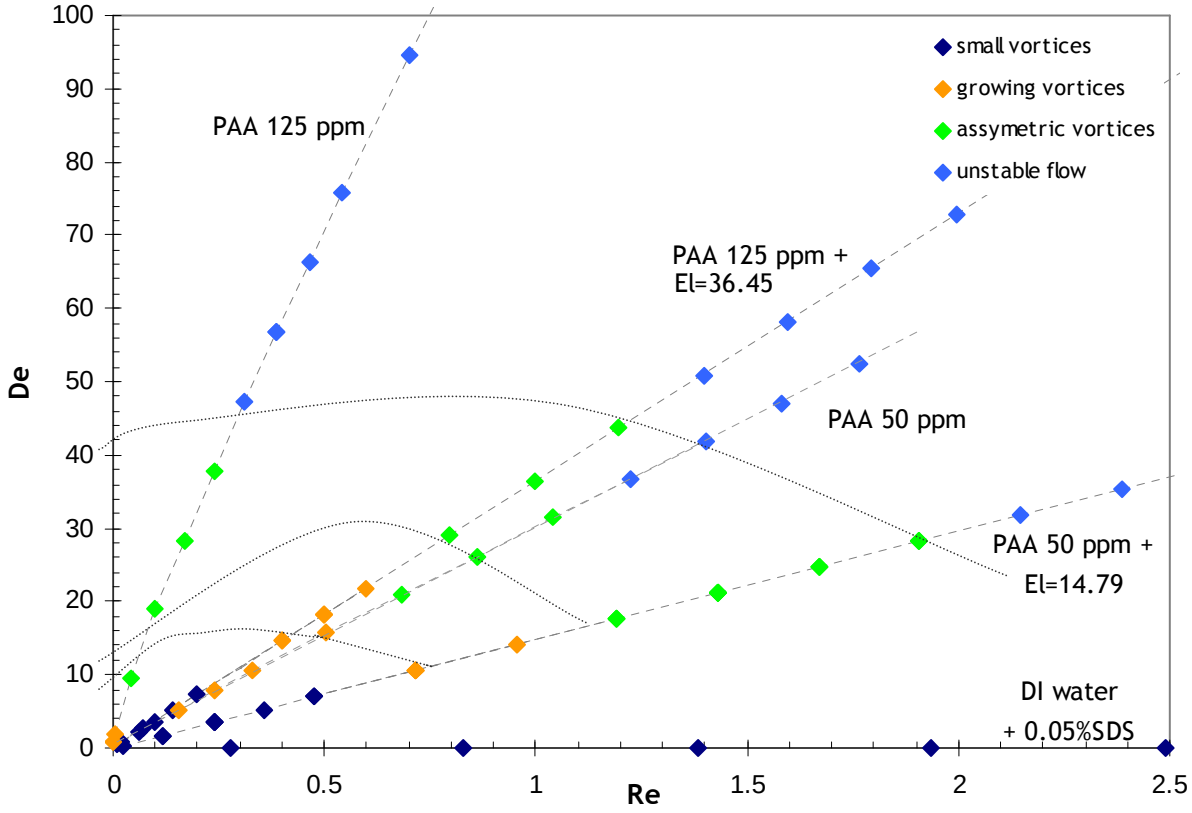

Figure 4.18: De-Re flow pattern map for symmetric channels.

By defining the different flow patterns distinction between the Newtonian fluid (water) and non-Newtonian fluids (PAA fluids) needs to be made as is shown in Figures 4.18 and 4.19 below.

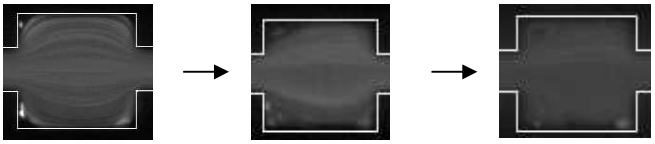

Figure 4.19: Flow patterns for the Newtonian fluid. (a) Small Moffatt vortices; (b) Vortex growth downstream of the expansion; (c) Further vortex growth downstream of the expansion vanishing vortices upstream of the contraction.

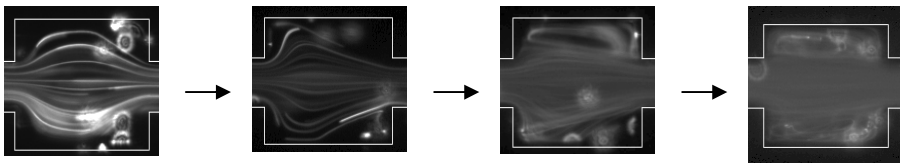

Figure 4.20: Flow patterns for non-Newtonian fluids. (a) Small corner vortices; (b) Symmetric vortex growth upstream of the contraction; (c) Asymmetric vortex growth; (d) Unstable flow

4.8.4.1 Deionized water

By flowing deionized (DI) water with 0.05% SDS at low flow rates small Moffatt vortices are observed. This is in agreement with the numerical predictions of Oliveira et al. (2008) for Newtonian fluids in two dimensional flows at low Reynolds numbers. Increasing the flow rate (*Re>10*, not shown in *De-Re* map) leads to growing vortices downstream of the expansion and reducing vortices upstream of the contraction, until they eventually vanish. Further increase leads to vanishing vortices of the upstream of the contraction and vortices downstream of the expansion remain growing. The same trend for Newtonian fluids has been observed in previous studies (Scott 2004; Rodd et al. (2005); Oliveira et al. 2008). At larger flow rates (not attained in the experiments) the vortex downstream of the expansion eventually increases until reaching the contraction plane and the main flow occurs only along the central region of the cavity.

4.8.4.2 Trends non-Newtonian fluids

In all used fluids a general trend is observed. For small flow rate used small Mofatt vortices or corner vortices are already visible upstream of the contraction. These vortices grow symmetrically with increasing *De*. Vortices downstream of the expansion reduce and eventually vanish. By increasing the flow rate the flows become asymmetric and steady. Increasing the flow even more resulted in unstable flow. Vortex growth is observed upstream of the contraction which is expected for viscoelastic fluids (Scott 2004; Rodd et al. 2005; Alves et al. 2005). In all the used fluids the same trend is observed. However, distinction can be made in the range and domain of *De* and *Re* in which the different flow patterns are observed. In the next sections the different flow regions for each fluid are discussed. The flow rate, Reynolds number and the Deborah number in the brackets give an indication of the boundaries of each region.

4.8.4.3 PAA 125 ppm with and without additives

For the PAA 125 ppm solution with additives small Mofatt vortices are observed at low flow rates (Q = 0.1 *ml/hr; Re* = 0.199; *De* = 7.27). At higher flow rates there is asymmetric vortex growth upstream of the contraction and the vortices downstream of the expansion vanish (Q = 0.2 ml/hr; *Re* = 0.399; *De* = 14.5). By increasing the flow rate (Q > 0.8 ml/hr) eventually the flow becomes unstable.

For the 125 ppm solution without additives the trend is the same, but at the lowest flow rate used (Q = 0.005 ml/hr; Re = 0.002; De = 0.95) asymmetric vortex growth upstream of the contraction is already observed. By increasing the flow rate (Q = 0.01 ml/hr; Re = 0.004; De = 1.90) vortices grow symmetrically upstream of the expansion. After that asymmetric steady vortices are observed and for Q > 0.2 ml/hr.

4.8.4.4 PAA 50 ppm with and without additives

For the 50 ppm solution without additives small vortices are observed at the lowest flow rate used (Q = 0.01 ml/hr; Re = 0.010; De = 0.52). After that the vortices grow upstream of the contraction (Q = 0.1 ml/hr; Re = 0.103; De = 5.24). At higher flow rates the flow becomes unstable and flipping vortices are observed (Q = 0.8 ml/hr; Re = 1.403; De = 41.9). For the solution with additives very small Mofatt vortices are observed at low flow rates (Q = 0.01 ml/hr; Re = 0.023; De = 0.35). Increasing the flow rate shows vortex growth upstream the contraction (Q = 0.3 ml/hr; Re = 0.716; De = 10.6). After that a large region of stable asymmetric vortices is observed (Q = 0.7; ml/hr; Re = 1.67; De = 24.7). Eventually the flow becomes unstable (Q = 1.5 ml/hr; Re = 3.58; De = 52.92).

4.8.4.5 Critical parameters

In the *De-Re* map (Figure 4.17) it is shown that different flow regimes are predicted. For $De \approx$ 0-8 only small vortices are observed. For $De \approx$ 10-20 a (symmetric) vortex growth regime is showed. By increasing Deborah number further an asymmetric vortex growth region is observed and eventually the flow becomes unstable ($De \rightarrow$ 30-40). However it can be seen that the behavior of PAA 125 ppm is different especially in the low flow regime. To understand this difference the relaxation time and elasticity of the fluids need to be mentioned. PAA 125 ppm has a relaxation time which is around 3 to 6 times larger than the relaxation time of the other fluids. This indicates that elastic effects are present in a greater extent. Furthermore a high relaxation time leads to large elasticity numbers as can be seen in Figure 4.21 where the elasticity number is plotted against Reynolds number. The reduction of El with Re occurs due to shear thinning of the shear viscosity.

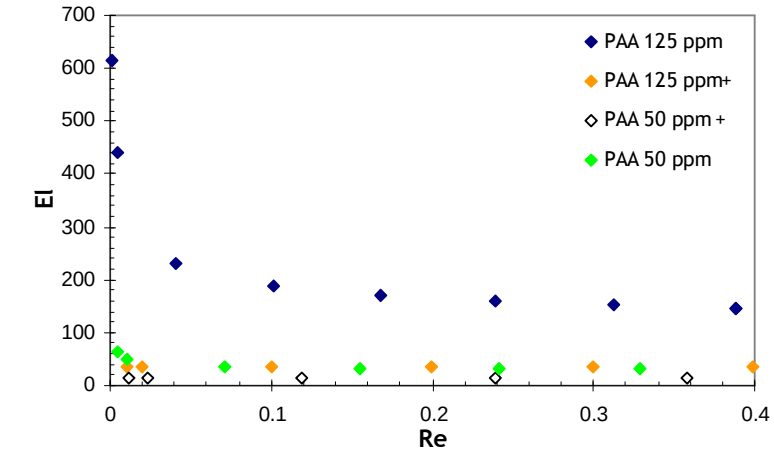

Figure 4.21: Elasticity number as function of Reynolds number for the fluids used.

At very low Reynolds numbers the elasticity number of PAA 125 ppm is very large compared to the other fluids. A very high elasticity number means that inertial effects are negligible compared to elastic effects. Therefore vortex growth and elastic effects are already observed at very low Reynolds numbers (*Re* → 0) for PAA 125 ppm. At higher Reynolds numbers the difference in elasticity number becomes smaller. This is also shown in the De-*Re* map since the critical Deborah number for unstable flow is similar to the same number of the other fluids.

4.9 Comparison of symmetric geometry with porous media

In order to compare the symmetric microchannel with a porous medium, first the particle size corresponding to the geometry of the microchannel is calculated (Figure 4.22 a). In the calculation an area of *2a* is used as an estimate for the hole between the particles (Figure 4.22 b). Then *a* is calculated by $a = 2W_c L_2 + W_1 L_1$ and *r* by $r = \sqrt{\frac{2a}{4 - \pi}}$. This gave a value of particles with a diameter (*2r*) of 337 µm. This diameter is compared with a diameter calculated by using the pressure drop data obtained in the experiments. Therefore Darcy's law is used to compare the obtained pressure data with pressure drop data of a porous medium. For the region in which a linear relationship of flow rate and pressure drop is observed the permeability is calculated using Equation 2.2.

The averaged calculated permeability for the symmetric geometry is around $1.3 \cdot 10^{-10}$ m^2. With this average permeability the diameter is calculated by $d = \sqrt{\frac{\kappa}{0.617 \times 10^{-11}}}$ (Krumbein and Monk 1943) with the permeability κ in cm^2 and d the diameter in µm. This resulted in a diameter of approximately 459 µm.

Since the results obtained from the pressure drop experimental data (d ≈ 459 µm) are similar to those estimated from a simple geometrical analysis (d ≈ 337 µm), this is an indication that the simple one-dimensional analogue of a porous media is a reasonable approximation.

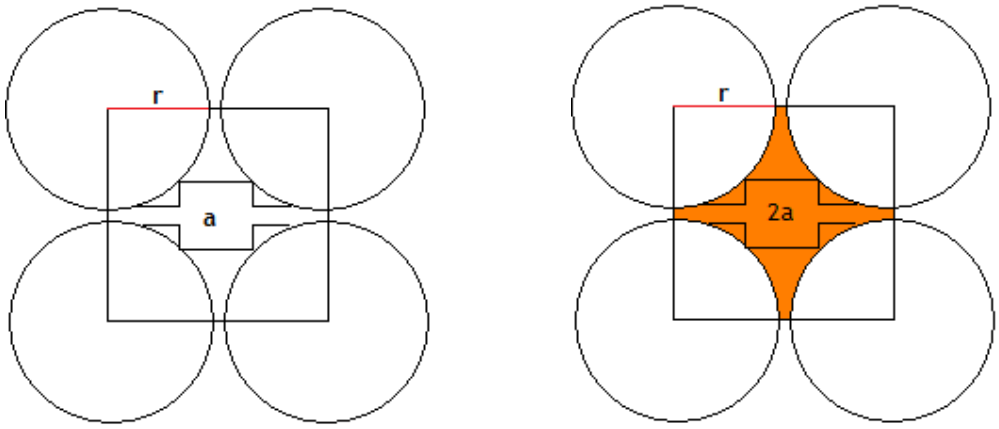

Figure 4.22: A symmetric geometry with surface area a surrounded by particles (spheres) with radius r (a) and the estimated surface of the entire hole between the particles (b).

5 Conclusions

Flows of water and diluted polyacrylamide aqueous solutions (50 and 125 ppm) through one-dimensional porous medium analogues were studied. For this purpose, microchannels with a symmetric and an asymmetric geometry were fabricated using soft lithography. In order to characterize the flow through the microchannels, visualizations of the flow patterns and pressure drop measurements were carried out. The influence of addition of 0.05 wt% SDS and 1 wt% NaCl on fluid and flow behavior was investigated.

Fluid characterization was done by studying the shear and extensional rheology of the used fluids. Shear viscosity measurements showed that addition of SDS and NaCl changes the rheological behavior of the solutions. Without additives a shear thinning behavior is observed. After addition of SDS and NaCl the shear viscosity is lowered significantly and remains almost constant over the whole range of applied shear rates. This behavior is similar to a Boger fluid. CaBER experiments showed also an influence of additives on the elasticity of the used fluids. Addition of additives lowers the relaxation time which indicates a lower elasticity.

In the asymmetric channel the polymer fluids show vortex growth upstream of the contraction. Only the flow of PAA 125 ppm becomes unstable at high flow rates (Q = 3.0 ml/hr). With DI water + 0.05 wt% SDS corner vortices downstream of the expansion grow slowly in the whole range of applied flow rates (Q = 0.1-9 ml/hr).

In the symmetric channel, a distinction between Newtonian and non-Newtonian fluids can also be made. With the Newtonian fluid (DI water + 0.05% SDS) small Mofatt vortices are observed at low flow rates. By increasing the flow rate, vortex growth downstream of the expansion is showed and vortices upstream of the contraction vanish. With the non-Newtonian fluids small vortices, symmetric and asymmetric vortex growth and finally unstable flow is observed.

Dimensionless numbers are used to define boundaries of the different flow regimes in the symmetric channel. For $De \approx$ 0-8 only small vortices are observed. For $De \approx$ 10-20 a (symmetric) vortex growth regime is showed. By increasing the Deborah number, first an asymmetric vortex growth region is observed and eventually the flow becomes unstable ($De \rightarrow$ 30-40). For PAA 125 ppm these boundaries deviate significantly at very low Reynolds numbers ($Re \rightarrow 0$). This can be explained by a higher relaxation time and elasticity numbers comparing to the other fluids.

In the pressure drop measurements of the fluids with additives a sudden pressure drop was observed at a critical flow rate. Visualizations showed that at this critical flow rate elastic instabilities arise. Without additives the relation of flow rate and pressure drop is quasi-linear. Here the viscous behavior suppresses the elastic behavior of the fluid. For water, the relation of flow rate and pressure drop is linear as expected for a Newtonian fluid.

Comparing the symmetric and asymmetric channels, it is clear that the former exhibits higher contraction/expansion ratios than the latter, which leads to a stronger extensional flow and a corresponding higher pressure drop. Furthermore, the critical flow rate at which the sudden pressure drop is observed is lower in the case of the symmetric channel.

Comparing the pressure drop data with Darcy's law showed that the symmetric microchannel can be seen as a good approximation to a porous medium analogue.

6 Evaluation of the work

6.1 Accomplished objectives

The goal of the project was to describe the flow of a dilute polymer solution through microchannels. First the fluid was characterized with rheological measurements. It turned out that addition of sodium chloride and SDS had a large influence on the rheological behavior of the fluids. Therefore four, instead of two, fluids were studied (PAA 125 and 50 ppm both with and without additives). Pressure drop measurements and visualizations gave a good insight in understanding the flow of the fluids through the microchannels. In the visualizations the symmetric channel was analyzed more intensively since they showed a more diverse behavior than the asymmetric channel. The comparison with a porous medium is only done in a small calculation and not carried out experimentally. Overall it can be concluded that the objectives of the project were accomplished.

6.2 Limitations and future work

In the project microchannels are used as analogue for a porous medium. In order to verify that the microchannel can be used as an analogue experiments in porous media need to be carried out. Pressure drop measurements of the used fluids through a column with a isotropic porous medium (particle size 300-400 μm) should give a good comparison with the pressure drop measurements done in this project. Furthermore the images obtained in the visualizations and the pressure drop results can be verified by performing simulations, which can then be used to extend the range of parameters studied.

6.3 Personal evaluation

In this project I learned a lot of new things. All the used techniques in the microchannel fabrication, pressure drop measurements and visualizations were new for me. Furthermore I learned how to participate in research and be in a laboratory for five days in a week. During the research I obtained a lot of data and I learned how to organize and analyze these data so that the important trends remained. I also learned that sometimes experiments do not work so patience and perseverance is required. At the end I learned how to write a report with the right lay-out and design. I liked to do this project and learn all these new things. I think in the future I will have much benefits of this half year research project.

References

Alves MA, Pinho FT, Oliveira PJ, Visualizations of Boger fluid flows in a 4:1 square–square contraction, AIChE Journal, **51**, 2908-2922 (2005).

Arratia PE, Thomas CC, Diorio JD, Gollub JP, Elastic instabilities of polymer solutions in extensional flows, Physical Review Letters, **96**, 144502 1-4 (2006).

Arrhenius SA, On the dissociation of substances dissolved in water, Zeitschrift fur Physikalische Chemie, **1**, 631–648 (1887).

Barnes HA, A handbook of elementary rheology, Instititute of Non-Newtonian Fluid Mechanics, University of Wales, Aberystwyth, Wales (2000).

Bassous E, Taub HH, Kuhn L, Ink jet printing nozzle arrays etched in silicon, Applied Physics Letters, **31**, 135-137 (1977).

Becker EW, Ehrfield W, Hagmann P, Maner A, Münchmeyer D, Fabrication of microstructures with high aspect ratios and great structural heights by synchrotron radiation lithography, galvanoforming, and plastic molding (LIGA process), Journal of Microelectronic Engineering, **4**, 35-56 (1986).

Becker H, Locascio LE, Polymer microfluidic devices: a review, Talanta, **56**, 267-287 (2002).

Bird RB, Carreau PJ, A nonlinear viscoelastic model for polymer solutions and melts, Chemical Engineering Science, **23**, 427-434 (1968).

Bird RB, Hassager O, Armstrong RC, Curtiss CF, Dynamics of polymeric liquids, John Wiley & Sons, New York, USA (1977).

Bogdanov AL, Peredkov SS, Use of X-ray lithography for very high aspect ratio X-ray lithography, Microelectronic Engineering, **53**, 493-496, (2000).

Boger DV, Highly elastic constant-viscosity fluid, Journal of non-Newtonian Fluid Mechanics, 1977, **3**, 87-91 (1977).

Brinkman HC, On the permeability of media consisting of closely packed porous particles. Applied Scientific Research, **1**, 81–86 (1947).

Brownlee G, Silverstein RM, A micro-preparative gas chromatograph and a modified carbon skeleton determinator, Analytical Chemistry, **40**, 2077-2079 (1968).

Bruus H, Theoretical Microfluidics, Oxford University Press, Oxford, UK (2008).

Bubendorfer A, Liu X, Ellis AV, Microfabrication of PDMS microchannels using SU-8/PMMA moldings and their sealing to polystyrene substrates, Smart Material Structures, **16**, 361-371 (2007).

Cross MM, Relation between viscoelasticity and shear-thinning behavior in liquids, Rheologica Acta, **18**, 609-614 (1979).

Dauben DL, Menzie DE, Flow of polymer solutions through porous media, Journal of Petroleum Technology, **19**, 1065-1073 (1967).

Darcy H, Les Fontaines Publiques de la Ville de Dijon, Dalmont, Paris (1856).

Entov VM, Hinch EJ, Effect of a spectrum of relaxation times on the capillary thinning of a filament of elastic liquid, Journal of non-Newtonian Fluid Mechanics, **72**, 31-54. (1997).

Ergun S, Fluid flow through packed columns. Chemical Engineering Progress, **48**, 9-94 (1952).

Evans RE, Walters K, Flow characteristics associated with abrupt changes in geometry in the case of highly elastic liquids, Journal of non-Newtonian Fluid Mechanics, **20**, 11-29 (1986).

Feng R, Farris RJ, Influence of processing conditions on the thermal and mechanical properties of SU-8 negative photoresist coatings, Journal of Micromechanics and Microengineering, **13**, 80-88 (2003).

Forchheimer P, Wasserbewegung durch Boden, Zeitsung Von Deutsche Ingenieurs, **45**, 1782-1788 (1901).

Ghannam MT, Rheological properties of aqueous polyacrylamide/NaCl Solutions, Journal of Applied Polymer Science, **72**, 1905-1912 (1998).

Groisman A, Enzelberger M, Quake SR, Microfluidic memory and control devices, Science, 300, 955-958 (2003).

Groisman A, Quake SR, A microfluidic rectifier: anisotropic flow resistance at low Reynolds numbers, Physical Review Letters, **92**, 1–4 (2004).

Haas R, Durst F, Viscoelastic flow of dilute polymer solutions in regularly packed beds, Rheologica Acta, **21**, 566-571 (1982).

Hai M, Han B, Study of interaction between sodium dodecyl sulfate and polyacrylamide by rheological and conductivity measurements, Journal of Chemical Engineering Data, **51**, 1498-1501 (2006).

Harper CA, Handbook of plastics, elastomers and composites (Table 1.21), Second edition, McGraw-Hill, New York (1992).

James DF, McLaren DR, The laminar flow of dilute polymer solutions through porous media, Journal of Fluid Mechanics, **70**, 733-752 (1975).

Kozicki W, Viscoelastic flow in packed beds or porous media, The Canadian Journal of Chemical Engineering, **79**, 124-131 (2000).

Krumbein WC, GD Monk, Permeability as a function of the size parameters of unconsolidated sands. Transaction of the American Institute of Mining, Metallurgical and Petroleum Engineers, **151**, 153-163 (1943).

Kullicke WM, Haas R, Flow behavior of dilute polyacrylamide solutions through porous media. 1. Influence of Chain Length, Concentration, and Thermodynamic Quality of the Solvent, Industrial and Enigneering Chemical Fundamentals, **23**, 308-315 (1984).

Li S, Freidhoff CB, Young RM, Ghodssi R, Fabrication of micronozzles using low-temperature wafer-level bonding with SU-8, Journal of Micromechanics and Microengineering, **13**, 732-738 (2003).

Liu G, Tian Y, Zhang X, Fabrication of microchannels in negative resist, Microsystem Technologies, **9**, 461-464 (2003).

Lorenz H, Despont M, Fahrni N, LaBianca N, Renaud P, Vettiger P, SU-8: a low-cost negative resist for MEMS, Journal of Micromechanics and Microengineering, **7**, 121–124 (1997).

Ma J, Cui P, Zhao L, Huang R, Synthesis and solution behavior of hydrophobic association water-soluble polymers containing arylalkyl group, European Polymer Journal, **38**, 1627-1633 (2002).

Marshall RJ, Metzner AB, Flow of viscoelastic fluids through porous media, Industrial and Engineering Chemical Fundamentals, **6**, 393-400 (1967).

McKinley GH, Rodd LE, Oliveira MSN, Justin Cooper-White J, Extensional flows of polymer solutions in microfluidic converging/diverging geometries, Journal of Central South University of Technology, **14**, 6-9 (2007).

Merkerk R, Ontwikkeling van de Lab on Chip technologie, Nano Ned, May, 1-3 (2005).

Nguyen H, Boger DV, The kinematics and stability of die entry flows. Journal of non-Newtonian Fluid Mechanics, **5**, 353-368 (1979).

Nguyen T, Wereley S, Fundamentals and applications of microfluidics, Integrated microsystems series, Second Edition, Artech House, Boston, USA (2006).

Oliveira MSN, Rodd LE, McKinley GH, Alves MA, Simulations of extensional flow in microrheometric devices, Microfluidics and Nanofluidics, **5**, 809-826 (2008).

Peckerar MC, Moldanado JR, X-ray lithography, an overview, Proceedings of the IEEE, **81**, 1249- 1274 (1993).

Penott-Chang EK, Gouveia L, Fernández IJ, Müller AJ, Díaz-Barrios AD, Sáez AE , Rheology of aqueous solutions of hydrophobically modified polyacrylamides and surfactants, Colloids and Surfaces A: Physicochemical and Engineering Aspects, **295**, 99-106 (2007).

Raha S, Williams M, Lamb P, Cone and plate rheometer for polymer melts, Journal of Physics E: Scientific Instruments, **1**, 1113-1115 (1968).

Raju R, Roy S, Hydrodynamic model for microscale flows in a channel with two 90 degrees bends, **126**, 489-493 (2004).

Rodd LE, Scott TP, Boger DV, Cooper-White JJ, McKinley GH, The inertio-elastic planar entry flow of low-viscosity elastic fluids in micro-fabricated geometries. Journal of non-Newtonian Fluid Mechanics, **129**, 1–22 (2005).

Rodd LE, Cooper-White JJ, Boger DV, McKinley GH, Role of the elasticity number in the entry flow of dilute polymer solutions in micro-fabricated contraction geometries, Journal of non-Newtonian Fluid Mechanics, **143**, 170-191 (2007).

Rothstein JP, McKinley GH, Extensional flow of a polystyrene Boger fluid through a 4:1:4 axisymmetric contraction/expansion, Journal of Non-Newtonian Fluid Mechanics, **86**, 61-88 (1998).

Ryder JF, Yeomans JM, Shear thinning in dilute polymer solutions, Journal of Chemical Physics, **125** (2006).

Scott TP, Contraction/Expansion Flow of Dilute Elastic Solutions in Microchannels, Master thesis, Massachusetts Institute of Technology, Cambridge, Massachusetts, USA (2004).

Sdougos HP, Bussolari SR, Dewey CF, Secondary flow and turbulence in a cone-and-plate device, Journal of Fluid Mechanics, **138**, 379-404 (1984).

Seeton CJ, Viscosity–temperature correlation for liquids, Tribology Letters, **22**, 67-78 (2006).

Sorbie KS, Parker A, Clifford PJ, Experimental and Theoretical Study of Polymer Flow in Porous Media, SPE Reservoir Engineering, **2**, 281-304 (1987).

Sousa PC, Coelho PM, Oliveira MSN, Alves MA, Three-dimensional flow of Newtonian and Boger fluids in square–square contractions, Journal of non-Newtonian Fluid Mechanics, **160**, 122-139 (2009).

Sousa PC, Pinho FT, Oliveira MSN, Alves MA, Efficient microfluidic rectifiers for viscoelastic fluid flow, Submitted to Journal of non-Newtonian Fluid Mechanics (2010).

Srinivasan V, Pamula VK, Fair RB, An integrated digital microfluidic lab-on-a-chip for clinical diagnostics on human physiological fluids, Miniaturisation for chemistry, biology and bioengineering, **4**, 310-315 (2004).

Toner M, Irimia D, Blood on a chip, Annual Review of Biomedical Engineering, **7**, 77-103 (2005).

Weigl BH, Bardell RL, Cabrera CR, Lab on a chip for drug development, Advanced Drug Delivery Reviews, **55**, 349-377 (2003).

Whitesides GM, The origins and the future of microfluidics, Nature, **442**, 368-373 (2006).

Williams MF, Landel FL, Ferry D, The temperature dependence of relaxation mechanisms in amorphous polymers and other glass-forming liquids, Journal of the American Chemical Society, **77**, 3701–3707 (1955).

Xia Y, Whitesides GM, Soft-lithography, Annual Review of Material Science, **28**, 153-184 (1998)

Yilmaz N, Bakhtiyarov AS, Ibragimov RN, Experimental investigation of Newtonian and non-Newtonian fluid flows in porous media, Mechanics Research Communications, **36**, 638-641 (2009).

Zhang J, Tan KL, Hong GD, Yang LJ, Gong HQ, Polymerization optimization of SU-8 photoresist and its applications in microfluidic systems and MEMS, Journal of Micromechanics and Microengineering, **11**, 20-26 (2001).

Appendix A Test procedure for shear viscosity measurements

Before characterizing the rheological behavior of the fluids to be used, a set of tests was performed in order to establish reliable experimental procedures and assess the repeatability of the flow curves obtained using the controlled stress shear rheometer (Physica MCR 301). In Figure A.1, the measurements obtained at 20°C with different samples of a 20 ppm PAA solution are shown.

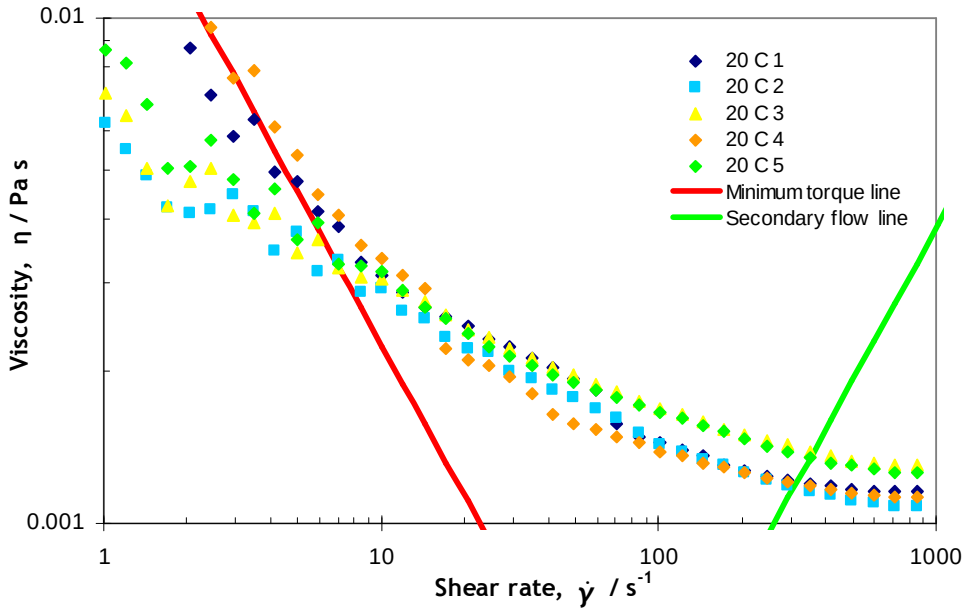

Figure A.1: Shear viscosity measurements with 20 ppm PAA (20°C).

As can be seen, the steady-shear viscosity curves are not overlapping and this should not happen. There are several factors which can influence the viscosity measurement:

- **Loading the fluid sample**

An incorrect volume of fluid used may result in a varying radius and eventually in a varying viscosity, since the shear viscosity (η) is calculated by:

$$\eta = \frac{\sigma}{\dot{\gamma}} = \frac{3M}{2\pi R^3}\frac{a}{\omega} \qquad (A.1)$$

where σ is the shear stress, $\dot{\gamma}$ the shear rate, *M* the torque and *R* and α are the radius and angle of the cone, respectively. In the calculations the gap between the cone and the plate is assumed to be totally filled. If the gap is underfilled the effective radius is smaller than that used in the calculations, resulting in a lower viscosity. A 1 mm difference in radius results in a 8.4% decrease of the viscosity. However, this effect would result in a constant off-set during the whole test, which is not the case (especially at low shear rates). Another factor which influences the viscosity if the plate is underfilled is the presence of air bubbles. Bubbles can come into the sample so instead of the viscosity of the fluid, the viscosity of the fluid with air bubbles is measured, which can exhibit large variations as bubbles are trapped and disappear as the measurement progresses.

On the other hand, overfilling will have an influence through the moment of inertia which is used to correct the viscosity (Pollice et al. 1982). When filling the plate, drops of fluid can fall on top of the cone resulting in a higher mass and subsequently a higher moment of inertia. This will not be corrected since the moment of inertia is calibrated before the gap is filled.

- **The time which is taken to achieve a uniform temperature.**

After loading the sample, the time should be long enough to achieve a uniform temperature. Otherwise, the actual temperature can differ from the required one resulting in a lower or a higher viscosity. If times are too long, evaporation can occur which can result in underfilling and in a higher concentration of polymer in the sample resulting in a higher viscosity. Since the sample is added in a thin layer a few minutes should be sufficient to start the measurements.

- **The time which is taken to obtain a steady value.**

A logarithmic duration scale was chosen, with higher duration for low shear rates and lower duration for high shear rates. Probably the times chosen were too low at the start of the measurements so a steady state was not obtained, resulting in different values of viscosity. To avoid this problem, duration limits were not imposed.

In order to make the measurement procedures more reliable particular attention was paid on filling the plate correctly and allowing the sample to reach a uniform temperature. The set of parameters used for the final measurements presented throughout this thesis are listed in Table A.1 under the heading “second set”.

Table A.1: Parameters used in shear viscosity measurements.

	First set of parameters	Second set of parameters
Variable	shear rate $\dot{\gamma}$ (s^{-1})	shear rate $\dot{\gamma}$ (s^{-1})
variable range	0.01 – 5000	0.1-5000
variable profile	ramp log	Ramp log
measured points	75	50
measuring points profile	duration log	no time setting
initial point	180 s	-
final point	5 s	-
total duration time	3707 s	-

Appendix B Important equations used in the calculation of the shear viscosity using a shear rheometer with a cone-and-plate or a plate-plate fixture

The shear rate is given by:

$$\dot{\gamma} = \frac{v}{h} \tag{B.1}$$

where $\dot{\gamma}$ is the shear rate (s^{-1}), h the height of the gap(m) and v the velocity (m/s) given by:

$$v = \omega r \tag{B.2}$$

where ω is the angular velocity (rad/s) and r is the radial distance from the center of the cone or of the plate center depending on the geometry used (m)

In a cone-and-plate geometry the height varies with r as:

$$h = r \tan a \tag{B.3}$$

with a the angle (rad). So, for small angles, the shear rate is given by:

$$\dot{\gamma} = \frac{r\,\omega}{r \tan a} = \frac{\omega}{a} \tag{B.4}$$

and the shear rate is place independent.

In a plate-plate geometry the height is the same everywhere. Therefore the shear rate in a plate-plate geometry is given by:

$$\dot{\gamma} = \frac{\omega\, r}{h} \tag{B.5}$$

and the shear rate depends on the radial distance r.